Journal of Structural Geology 31 (2009) 1322–1339

Contents lists available at ScienceDirect

Journal of Structural Geology

journal homepage: www.elsevier.com/locate/jsg

Clast-based kinematic vorticity gauges: The effects of slip at matrix/clast interfaces

Scott E. Johnson [a,*], Hendrik J. Lenferink [a,1], Nancy A. Price [a], Jeffrey H. Marsh [a], Peter O. Koons [a], David P. West Jr. [b], Rachel Beane [c]

[a] Department of Earth Sciences, University of Maine, Orono, ME 04469, USA
[b] Department of Geology, Middlebury College, Middlebury, VT 05753, USA
[c] Department of Geology, Bowdoin College, Brunswick, ME 04011, USA

ARTICLE INFO

Article history:
Received 29 January 2009
Received in revised form
7 July 2009
Accepted 30 July 2009
Available online 4 August 2009

Keywords:
Kinematic vorticity number
Clast rotation
Mica fish
Numerical modeling
Viscosity contrast
Mylonite
Shear zone

ABSTRACT

Clast-based methods for estimating the mean kinematic vorticity number W_m are compromised by strain localization at the clast margins. Localization increases with modal matrix mica content as determined with samples from the Sandhill Corner mylonite zone – a crustal-scale, high-strain, strike-slip shear zone in Maine. Using these samples, we estimate W_m with the oblique quartz shape-preferred orientation and rigid-clast rotation methods. The rigid-clast rotation method yields much lower values for W_m than the quartz method. To investigate whether or not slip at the matrix/clast interface can explain the discrepancy in calculated W_m, we conducted numerical modeling of rigid clasts enveloped by a low viscosity layer, both embedded within a shearing viscous matrix. Within this dynamic framework, we carried out numerical sensitivity analyses in which we varied the viscosity ratio between the lubricating layer and the surrounding matrix, the thickness of the lubricating layer, and the kinematic vorticity number of the bulk flow. Our data and numerical results succeed in explaining why W_m estimates from clast-based rotational methods are typically lower than estimates from other methods, and this has implications for testing hypotheses related, for example, to vorticity partitioning in oblique convergent settings, crustal-scale extrusion or channel flow, and exhumation of ultra-high pressure rocks, all of which rely on robust estimates of W_m. The relation between the shape preferred orientations of clasts and modal mica content lead to the hypothesis that mica is the cause of the lubrication at clast/matrix interfaces. If so, then we surmise that mica fish should be self-lubricating and would therefore form an end-member shape preferred orientation, regardless of matrix modal mica content. The unique role of mica allows us to speculate about the bounds on viscosity contrast between the matrix and lubricated clast interfaces.

1. Introduction

Ancient orogens provide information about how deformation in active orogens is distributed and accommodated at depth, which is important for modern concepts about how deformation is coupled across the frictional-to-viscous transition (e.g., Handy et al., 2007). Studying rocks from ancient orogens that were deformed in viscous flow at depth requires indirect techniques for estimating kinematic flow parameters. The most widely used method for estimating these parameters is the microstructural determination of kinematic vorticity number (reviewed below). The problem is that microstructural vorticity gauges commonly give a wide range of values from samples collected in close proximity to one another, and different methods can give markedly different results when applied to the same rock. These variations are troublesome because robust estimates of kinematic vorticity are important for testing hypotheses related, for example, to vorticity partitioning in oblique convergent setting (e.g., Holcombe and Little, 2001; Short and Johnson, 2006), lower-crustal extrusion or channel flow (e.g., see references in Law et al., 2006), and the exhumation of ultra-high pressure rocks (e.g., Marques et al., 2007).

In this paper, we investigate the effects of strain localization at clast margins on the value of the kinematic vorticity number as determined by the rigid clast rotation method. In the following section we review the instantaneous kinematic vorticity number W_k, and two methods for estimating the mean kinematic vorticity

* Corresponding author. Fax: +1 207 581 2202.
E-mail address: johnsons@maine.edu (S.E. Johnson).
[1] Current address: Department of Earth, Atmospheric and Planetary Sciences, Massachusetts Institute of Technology, Cambridge, MA 02139, USA.

0191-8141/$ – see front matter © 2009 Elsevier Ltd. All rights reserved.
doi:10.1016/j.jsg.2009.07.008

number W_m: the oblique quartz shape-preferred orientation and rigid clast rotation methods. One of our goals is to compare these two methods in a number of samples and explore explanations for why they differ so markedly. In order to test methods for estimating W_m, we require a field area that meets certain kinematic criteria. We introduce the Sandhill Corner mylonite zone, which is the largest mylonitic strand in the Norumbega Fault System, northern Appalachians, Maine (Ludman and West, 1999). A case is made that this vertical, high-strain, strike-slip shear zone experienced approximately plane-strain, monoclinic flow. We then show the results of analyses on six samples from this shear zone. The results of these analyses are followed by numerical modeling where we explore the stable positions of lubricated clasts across a range of W_k. Our findings lead us to explore other ways in which lubricated clast data can be used to estimate the kinematic vorticity number. Our findings also provide a better understanding of mica fish and allow us to speculate about the bounds on viscosity contrast between the matrix and lubricated clast interfaces.

2. The kinematic vorticity number (W_k) and mean kinematic vorticity number (W_m)

2.1. Definitions and assumptions

The kinematic vorticity number, W_k, is defined as

$$W_k = w\left[2(s_1^2 + s_2^2 + s_3^2)\right]^{-\frac{1}{2}} \quad (1)$$

where w is the magnitude of the vorticity vector and the s_i are the principal stretching rates (Means et al., 1980; Passchier, 1987; Tikoff and Fossen, 1993). W_k first appeared in fluid dynamics literature (Truesdell, 1953) and was later introduced into geological literature by McKenzie (1979) and Means et al. (1980). W_k is a measure of the non-coaxiality of flow, denoting the relative rates of rotation and stretching at a point in space and a moment in time. Alternatively, W_k is a dimensionless ratio where the numerator is the instantaneous rate at which material lines parallel to the instantaneous stretching axes (ISAs) are rotating with respect to those axes and the denominator is the instantaneous rate at which those same material lines are being stretched along the same axes (Means et al., 1980). Flow types in a reference frame fixed to the ISAs range from pure shear ($W_k = 0$) to simple shear ($W_k = 1$), with intermediate types referred to as general non-coaxial flow ($0 < W_k < 1$). The reference frame is critical when assessing W_k. As discussed by Simpson and De Paor (1993), theoretical treatments typically use the ISAs as the reference frame. However, when applied, geologists must use some visible markers such as shear zone boundaries or a foliation. In high strain mylonites, such as the Sandhill Corner mylonite zone, the boundaries of the shear zone are typically impossible to define precisely, so it is useful to begin with the mylonitic foliation as the reference frame. For monoclinic, plane-strain deformation, W_k is a function of the acute angle α between the non-vanishing velocity field eigenvectors (flow apophyses AP_1 and AP_2 in Fig. 1) in the plane containing ISA_1 and ISA_2 (Bobyarchick, 1986; Passchier, 1986):

$$W_k = \cos(\alpha) \quad (2)$$

If strains are very large, the foliation may be approximately parallel to AP_1, which is theoretically parallel to the shear plane (Fig. 1). However, they can never be exactly parallel. To ensure that the flow plane is the externally fixed reference frame, the angle δ between the foliation and AP_1, determined using quartz c-axis pole figures (Fig. 2), should be added as a correction factor.

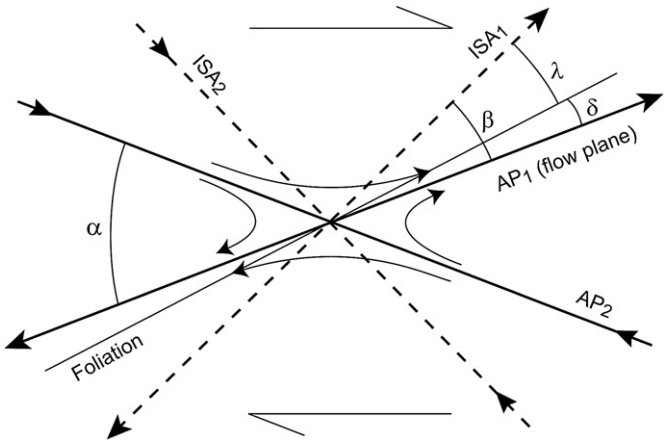

Fig. 1. Diagram of 2D monoclinic flow kinematics. All proceeding figures assume this frame of reference. ISA_1 and ISA_2 denote instantaneous stretching axes. AP_1 and AP_2 denote velocity field eigenvectors or flow apophyses. Arrowed curves represent flow lines. For plane-strain (2D) deformation, the angle α defines the non-coaxiality of flow ($W_k = \cos(\alpha)$). Single-sided arrows indicate top-to-the-right sense of shear. The relationships between β, λ and δ are described in Eq. (5).

The use of W_k in a geological setting is facilitated when the vorticity vector is perpendicular to the plane containing the instantaneous stretching axes, which requires strain to have monoclinic or orthorhombic symmetry. Iacopini et al. (2007b) argued that strain symmetry cannot be markedly triclinic in rocks that record high W_k values and show well-developed fabrics, so strain in such rocks may approach monoclinic or orthorhombic symmetry. In order to define W_k in the range $0 \le W_k \le 1$ for pure to simple shear, strain must strictly be 2D. However, Tikoff and Fossen (1995, fig. 5) showed that divergence from plane strain has only a small effect on W_k ($\Delta W_k \le 0.05$) for specific reference deformations.

Owing to the instantaneous nature of W_k, assumptions about the kinematics must take into account possible changes in boundary conditions over time. Recognizing that flow may be non-steady, varying in time and space, Passchier (1987) suggested that the kinematic vorticity number extracted from rocks be called the mean kinematic vorticity number (W_m) and viewed as a parameter of finite as opposed to instantaneous deformation (see also Fossen and Tikoff, 1998, and Jiang, 1998, for references). Below, we use both W_k and W_m, depending on the context.

Like most techniques used in field-based analyses, kinematic vorticity analysis has important limitations and care is required when selecting sites and samples for application. The results of kinematic vorticity analyses can provide quantitative information if: (a) the rocks being examined have experienced moderate to high strains, (b) the rocks show very strong fabric development, (c) the strain symmetry deviates only moderately from plane monoclinic, and (d) there is no evidence to contradict an assumption of approximately steady long-term flow. Thus, the accuracy of the analysis will depend on the methods used and how well these methods record W_k.

2.2. Background on estimation and application of W_m

Several different methods have been established for estimating W_m from deformed rocks (see reviews in Simpson and De Paor, 1993; Tikoff and Fossen, 1995; Wallis, 1995; Law et al., 2004; Passchier and Trouw, 2005), and these have been extensively applied to both active and ancient zones of deformation (e.g., Passchier, 1987; Vissers, 1989; Wallis et al., 1993; Wallis, 1992, 1995; Masuda et al., 1995; Simpson and De Paor, 1997; Beam and Fisher, 1999; Grasemann et al., 1999; Xypolias and Doutsos, 2000;

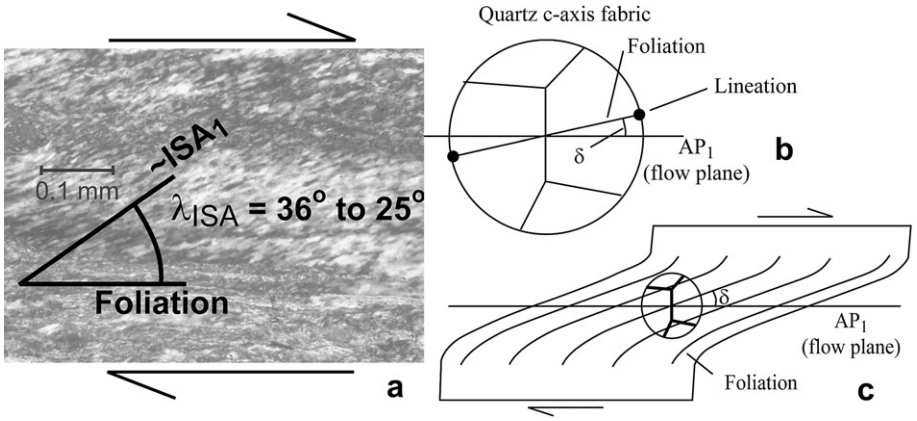

Fig. 2. Essentials of the oblique quartz shape-preferred orientation method for estimating W_k. (a) 'Snapshot' at the last increment of deformation in the SCMZ: new quartz grains are initially stretched in the direction of ISA_1 and then rotate progressively towards the shear plane (AP_1), which in this example is approximately parallel to the foliation. The angle λ_{ISA} between the foliation and new grains, which varies by $>10^\circ$ in this image, contains information about W_m. (b) Schematic fabric skeleton of quartz c-axis data showing a cross-girdle pattern. AP_1 is theoretically perpendicular to the central girdle marked by the central stick in the fabric skeleton. The angle δ is obtained by measuring the angle between the foliation and the line perpendicular to the central stick. (c) Generalized diagram placing the quartz pole figure into a shear-zone context.

Holcombe and Little, 2001; Xypolias and Koukouvelas, 2001; Bailey and Eyster, 2003; Bailey et al., 2004, 2007; Giorgis and Tikoff, 2004; Law et al., 2004; Carosi et al., 2006; Jessup et al., 2006, 2007; Xypolias and Kokkalas, 2006; Forte and Bailey, 2007; Iacopini et al., 2007a; Marques et al., 2007; Sullivan, 2008; Xypolias, 2009). Notable recent examples include testing orogen-scale models for channel flow or ductile extrusion (e.g., Grasemann et al., 1999; Law et al., 2004; Carosi et al., 2006; Jessup et al., 2006; Williams et al., 2006; Xypolias and Kokkalas, 2006) and characterizing the flow parameters associated with the exhumation of high- and ultra-high pressure rocks (e.g., Marques et al., 2007).

The most widely used technique for estimating W_m is the rigid clast rotation method of Passchier (1987) and Wallis et al. (1993), which involves measuring the stable orientations of relatively large, rigid minerals in a finer-grained, flowing matrix. A problem we have encountered in evaluating our own and other published data is that clast orientations commonly cluster in positions not predicted for viscous coupling of a single-phase Newtonian matrix and a rigid clast (e.g., Arbaret et al., 2001; Pennacchioni et al., 2001; ten Grotenhuis et al., 2002; Mancktelow et al., 2002; Ceriani et al., 2003; Marques et al., 2007). In addition, a number of studies have noted that the clast method commonly gives W_m values that are much lower than those values determined by other methods applied to the same rocks (e.g., Wallis, 1995; Bailey and Eyster, 2003; Law et al., 2004; Jessup et al., 2006; Xypolias and Kokkalas, 2006; Sullivan, 2008). Analog (e.g., Ildefonse and Mancktelow, 1993; Mancktelow et al., 2002; ten Grotenhuis et al., 2002; Ceriani et al., 2003) and numerical (e.g., Kenkmann and Dresen, 1998; Marques et al., 2005a,b; Schmid and Podladchikov, 2005; Johnson, 2008) models show that where strain localization occurs at the clast interface, stable clast orientations change, sometimes rotating progressively backward against the flow. This provides a possible explanation for observed data trends (e.g., Marques et al., 2007). Previously published numerical studies do not include W_k as a variable in sensitivity analyses, although one analytical solution (Mulchrone, 2007) predicts W_k values from clast orientations where total slip occurs at the interface between a clast and single-viscosity Newtonian matrix.

3. Selected microstructural methods for estimating W_m in this study

A number of microstructural methods can be applied to estimate W_m in rock samples, and these have been thoroughly reviewed, for example, by Wallis (1992, 1995), Tikoff and Fossen (1995), Law et al. (2004) and Passchier and Trouw (2005). These methods include: (1) the oblique quartz shape-preferred orientation (SPO) method of Wallis (1995), (2) the rigid clast rotation method of Passchier (1987) and Wallis et al. (1993), (3) the porphyroclast hyperbolic distribution method of Simpson and De Paor (1993, 1997), and (4) the quartz strain ratio method of Wallis (1992, 1995). In the Sandhill Corner mylonite zone, the oblique quartz shape-preferred orientation and rigid clast rotation methods are widely applicable. In contrast, well-developed recrystallized tails must be present around clasts to successfully employ the porphyroclast hyperbolic distribution method, and our observations so far show that such tails are only locally present. Grasemann et al. (1999, fig. 10b) showed that the quartz strain ratio method is unreliable in high-strain samples ($R_{xz} > 10$–15) and, given the very high strains apparent in the SCMZ, this method is unlikely to give valid results. Below we summarize only the two methods that are most widely applicable in our rocks.

3.1. Method 1: oblique quartz shape-preferred orientation

For plane-strain flow, if β is the acute angle between the instantaneous stretching axis ISA_1 and flow apophysis AP_1 (Fig. 1), then:

$$\beta = \frac{1}{2}(90^\circ - \alpha) \tag{3}$$

$$W_m = \sin(2\beta) \tag{4}$$

The aim of this method is to determine β. During deformation, new, dynamically recrystallized quartz grains are stretched in the direction of ISA_1 (Fig. 2a). With increasing strain, they progressively deform and rotate towards AP_1 leading to c-axis pole figures typically characterized in our rocks by single- and cross-girdle patterns (Fig. 2b) that are consistent with fabrics predicted by numerical models (e.g., Lister and Hobbs, 1980; Wenk et al., 1989; Jessell and Lister, 1990; Takeshita et al., 1999) and observed in high $P-T$ deformation experiments (e.g., Tullis et al., 1973; Tullis, 1977; Heilbronner and Tullis, 2002) in plane-strain conditions. The central segment of the c-axis girdle is expected to lie at right angles to AP_1 in both simple shear (e.g., Law, 1990; Lister and Hobbs, 1980) and general monoclinic shear (e.g., Platt and Behrmann, 1986; Vissers, 1989; Wallis et al., 1993).

If λ_{ISA} is the maximum angle between the foliation and ISA_1 as inferred from dynamically recrystallized quartz grains (Fig. 2a), and δ is the angle between the foliation and the normal to the central girdle of the quartz c-axis pattern (AP_1, Fig. 2b, c), then:

$$\beta = \lambda_{ISA} + \delta \tag{5}$$

$$W_m = \sin(2\lambda_{ISA} + 2\delta) \tag{6}$$

3.2. Method 2: rigid clast rotation

The rigid clast rotation method exploits the rotational behavior of relatively large rigid clasts in high-strain deformed rocks such as mylonites. The cross-sectional shape and orientation of a clast is approximated as an ellipse (Fig. 3a) with θ marking the angle between the major axis and AP_1, and with the major and minor axes (m_i) typically expressed as the aspect ratio ($R = m_1/m_2$) or cross-sectional shape factor ($B = (m_1^2 - m_2^2)/(m_1^2 + m_2^2)$). Although published studies take θ as the angle between the major clast axis and the foliation plane, the angle should be corrected where possible, as in Method 1, by adding the angle δ from the quartz c-axis pole figures (Figs. 1b and 2b). This correction (resulting in the angle β in Fig. 1) will not change the B cutoff value traditionally used to estimate W_m, but it will change the θ amplitude, a point that will become important later in this paper.

Jeffery's (1922) theory predicts that ellipsoidal rigid particles in a Newtonian viscous medium undergoing simple shear rotate synthetically (forward with respect to the sense of shear) as a function of B, θ, and the shear strain rate $\dot{\gamma}$. Using pioneering analog models, Ghosh and Ramberg (1976) studied the rotational behavior of such particles in general non-coaxial flow ($0 < W_k < 1$) and derived an equation describing their rate of rotation:

$$\dot{\theta} = \frac{\dot{\gamma}}{2}\left[1 - B\cos(2\theta) - \frac{B}{W_k}\sqrt{1 - W_k^2}\sin(2\theta)\right] \tag{7}$$

Particles with shape factors above a critical value (B_{crit}) rotate towards and asymptotically approach a stable orientation θ_s, whereas rounder particles rotate continuously in the flow. The stable orientation is sensitive to B and W_k (Passchier, 1987):

$$\theta_s = -\frac{1}{2}\sin^{-1}\left\{\frac{W_k}{B}\left(\sqrt{1 - W_k^2} - \sqrt{B^2 - W_k^2}\right)\right\} \tag{8}$$

Particle rotation also ceases at a second, metastable orientation θ_m for those particles more elongate than the critical shape factor:

$$\theta_m = \frac{1}{2}\sin^{-1}\left\{\frac{W_k}{B}\left(\sqrt{1 - W_k^2} - \sqrt{B^2 - W_k^2}\right)\right\} - \frac{1}{2}\sin^{-1}\left(\sqrt{1 - W_k^2}\right) \tag{9}$$

The acute angle between the metastable and stable particle orientations ($\theta_m < \theta < \theta_s$) defines a field of antithetic (backward) rotation; the remaining range ($\theta_s < \theta < \theta_m$) defines a field of synthetic (forward) rotation. The metastable orientation is transient and is rarely observed in experimental and natural examples.

The stable orientation (Eq. (8)) enables a method for estimating the mean kinematic vorticity number W_m. In theory, there is a sharp transition between the shape-preferred orientation (SPO) of clasts more elongate and less elongate than the critical shape factor B_{crit} (Fig. 3c). The critical shape factor B_{crit} records W_m (Passchier, 1987):

$$W_m = B_{crit} = \frac{R_{crit}^2 - 1}{R_{crit}^2 + 1} \tag{10}$$

4. Details of the study area

4.1. Background and description

Testing methods for estimating W_m requires a geologic setting wherein the respective crystallographic and SPO fabrics are well-developed and well-preserved. The area must also preserve approximately monoclinic, steady-state deformation. Below we establish the Sandhill Corner mylonite zone (SCMZ) in the south-central portion of the Norumbega Fault System (NFS, Fig. 4) as a suitable field locality for conducting these studies.

The NFS represents the roots of a long-lived, Paleozoic, right-lateral, large-displacement, subvertical, plate-boundary-parallel fault system (Ludman et al., 1999; West, 1999; Wang and Ludman,

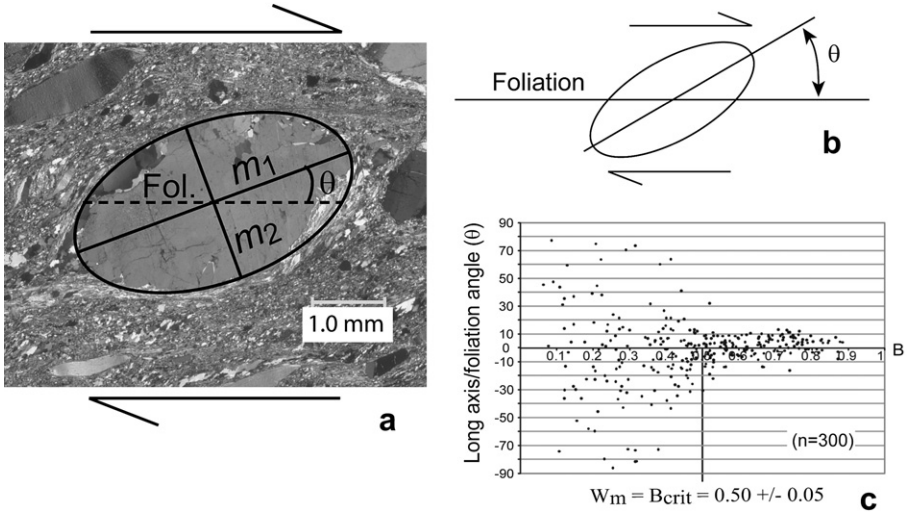

Fig. 3. Essentials of the rigid clast rotation method for estimating W_m. (a) A best-fit ellipse approximates the cross-sectional shape of a feldspar porphyroclast with major and minor axes (m_i), shape factor B, and orientation θ relative to the foliation (dashed horizontal line). Note the mica fish in the upper-left of the image. (b) Line diagram showing θ, the angle between the long axis of the clast and the foliation. (c) A plot of 300 measurements of θ versus B (sample H12). The vertical line at $B = 0.50 \pm 0.05$ identifies the critical B value separating clasts that continuously forward rotate ($B < B_{crit}$) from clasts that reach a stable orientation ($B > B_{crit}$). This cutoff value is traditionally taken as W_m.

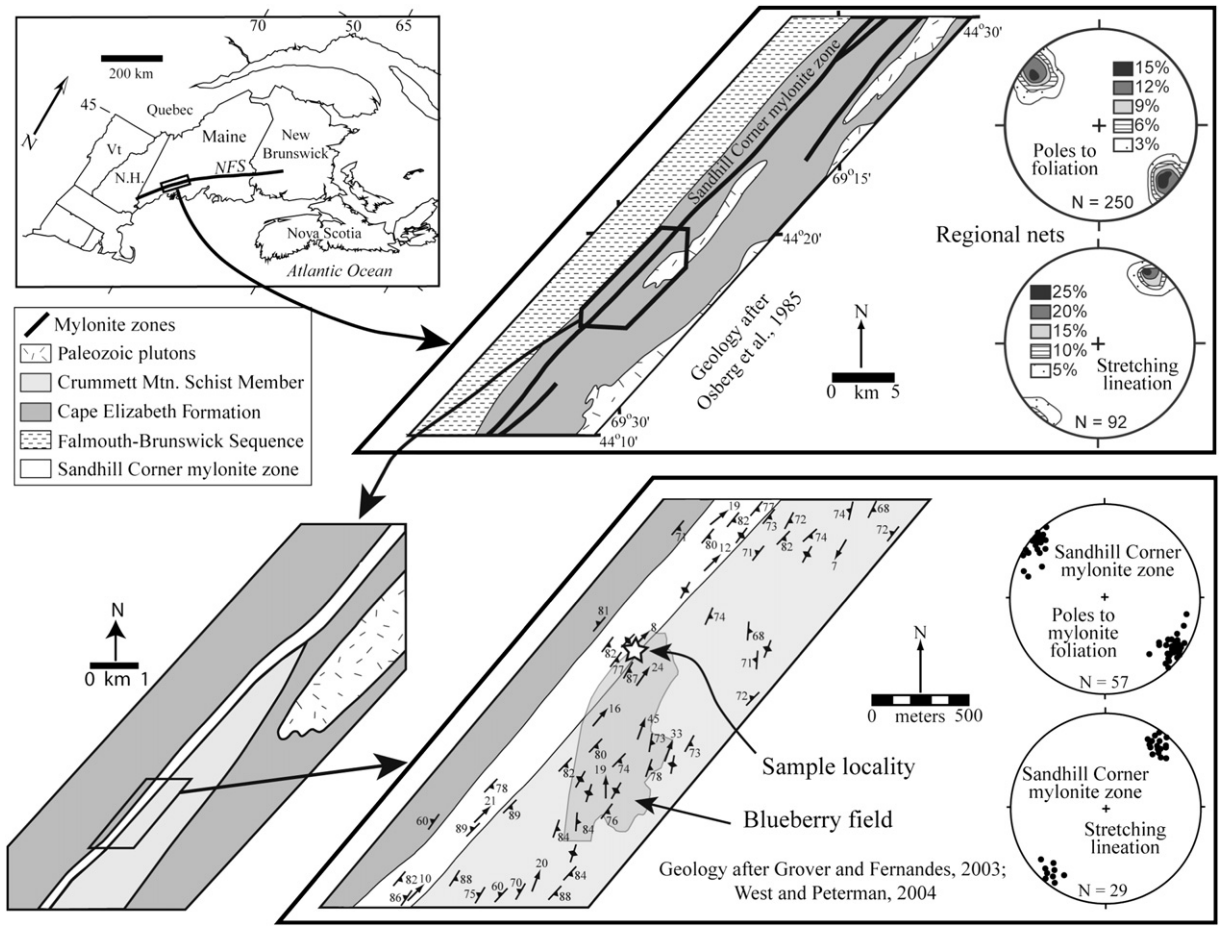

Fig. 4. Geologic map of the study area within the Norumbega Fault System. Equal area nets at upper right include mylonitic and non-mylonitic rocks of the broader Norumbega Fault System in the map area shown. Detailed map at lower right shows that foliation and lineation orientations in the SCMZ are identical to the regional orientations. Samples for this study come from the area marked by the star, at the northern edge of a large blueberry field. (Osberg et al., 1985).

2003). Both the width and length of the NFS are similar to those of the San Andreas system (Ludman and West, 1999), and seismic reflection data show vertical fault disruption down through the Moho (Doll et al., 1996). Detailed mapping and structural studies were completed along the southwestern (e.g., Swanson, 1988, 1989, 1999, 2005, 2006), central (e.g., West and Hubbard, 1997; Hubbard and Wang, 1999; Short and Johnson, 2006), and northeastern (e.g., Ludman, 1998; Wang and Ludman, 2004) segments of the NFS. The work we present here was conducted in the SCMZ in south-central Maine, which we consider to be a suitable location for testing methods of estimating W_m for the following reasons.

(1) Recent 1:24,000 scale bedrock mapping (Grover and Fernandes, 2003; West and Peterman, 2004) shows that the SCMZ varies in width from 100 to 300 m, contains a subvertical foliation and subhorizontal stretching lineation, and shows a record of dextral strike-slip kinematics (Fig. 4).
(2) Quartz microstructures in the SCMZ show clear evidence for dislocation creep accompanied by dynamic recrystallization leading to a strong crystallographic preferred orientation. Thin, discontinuous bands and isolated pools of quartz with pronounced SPO oblique to the foliation are common (Fig. 2a) as are feldspar porphyroclasts (Fig. 3a).
(3) Recent low-temperature thermochronological work across the SCMZ shows no evidence for post-Paleozoic offset (West et al., 2008). Furthermore, these rocks show none of the evidence typical of low-temperature fault-zone reactivation, such as pervasive low-temperature fracturing and cataclasis. Thus, the mylonites appear to have been exhumed without appreciable deformational or thermal overprint.

4.2. Assumptions and justifications related to the field area

The key assumptions required for applying methods for estimating kinematic vorticity numbers in the SCMZ are that: (1) the strain symmetry is not markedly triclinic (e.g., Passchier, 1988, 1997, 1998; Robin and Cruden, 1994; Tikoff and Fossen, 1995, 1999; Fossen and Tikoff, 1998; Lin et al., 1998; Jiang et al., 2001), and (2) the deformation was near steady-state at the time the microstructural record was frozen in. The following evidence suggests approximately plane, monoclinic flow in the SCMZ.

(a) Equal area projections of foliations and lineations throughout the SCMZ (Fig. 4) resemble those for monoclinic plane strain with a significant component of simple shear as predicted by slip-line theory (Gapais and Cobbold, 1987).
(b) Quartz c-axis pole figures (Fig. 5; Hubbard and Wang, 1999) show both single and cross-girdle patterns with dominant maxima in the macroscopic foliation plane at right angles to the mineral lineation.

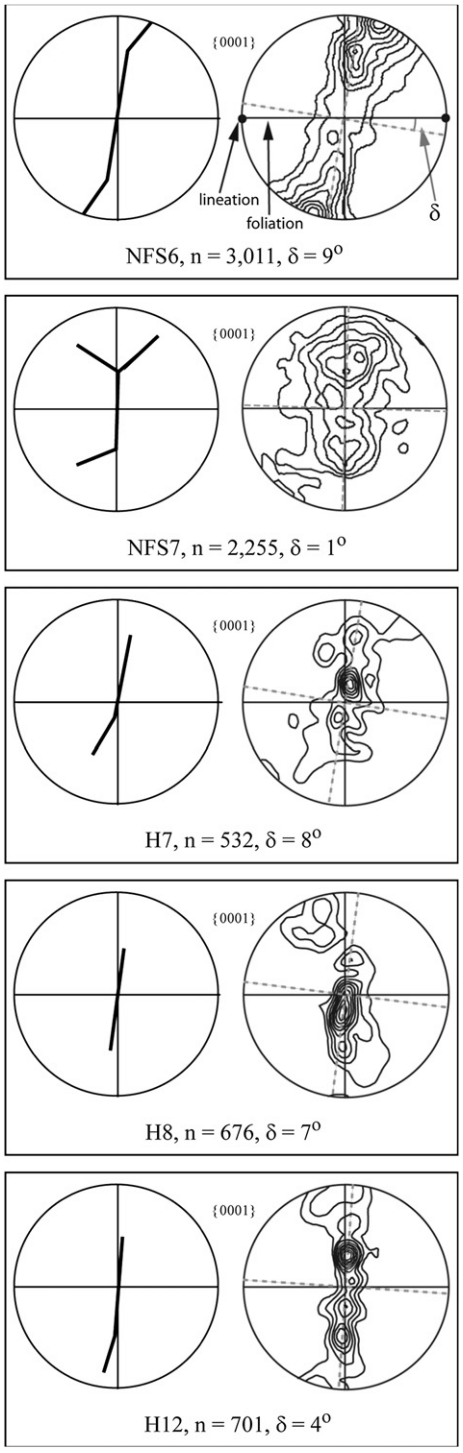

Fig. 5. Quartz c-axis pole figures from foliation-parallel quartz veins in five selected samples from the SCMZ. Each example includes sample information, a contoured quartz c-axis plot, and a fabric skeleton constructed manually from the contoured c-axis data. Pole figures are lower hemisphere equal area projection plots with contours set at mud (multiples of uniform density) values of, 1…10 and ± 0.25, 0.5,15, half width at 10°, and data clustering at 5°. Sense of shear is top-to-the-right in all figures, and the lineation lies in the plane of foliation, as shown on the c-axis plot for NFS6. The dotted grey lines show the orientation of the flow plane, which is normal to the cross girdle and oblique to the foliation to produce the angle δ. HKL-Channel 5 and TSL-OIM software were used to create the pole figures, and c-axis orientation data were collected using SEM-EBSD techniques (avg. MAD- 0.85° for HKL-Channel 5; avg. fit-1.29 and avg. confidence interval-0.25 for TSL-OIM).

(c) Foliations and lineations in the SCMZ are very well developed and W_m is apparently near 1.0 (analysis below), so any deviation from monoclinic symmetry is likely to be minor (Iacopini et al., 2007b).
(d) Pronounced asymmetry occurs in the foliation wrapping around rigid clasts in sections perpendicular to foliation and parallel to lineation. In contrast, the foliation wraps more symmetrically around clasts in the two mutually perpendicular sections (cf., Forte and Bailey, 2007).

The second assumption, that the microstructural record reflects steady long-term deformation, is never easy to justify. However, individual shear zones in fault systems coalesce to form interconnected weak horizons, and this process continues until the entire deformational system approaches steady creep at lower bulk strength than in its initial state (e.g., Handy, 1994; Ben-Zion and Sammis, 2003; Handy et al., 2007). Thus, mature faults/shear zones are more likely to preserve microstructures indicative of steady long-term flow than immature ones. Given the large shear strains accommodated by the SCMZ, an approach to steady state seems reasonable.

5. Data from the SCMZ

5.1. Quartz c-axis pole figures

Quartz c-axis pole figures are required to determine the angle δ between the foliation and AP_1 (Fig. 1). Quartz-rich volumes in the SCMZ occur primarily as thin, discontinuous, foliation-parallel veins and small, isolated pools. In order to acquire the appropriately large number of data points for c-axis pole figures, we selected foliation-parallel veins that appear optically to be fully dynamically recrystallized.

Samples were prepared as probe-quality thin sections with a mechanical polish to 0.3 μm followed by a chemical polish with colloidal silica suspensions (SYTON method of Fynn and Powell, 1979). NFS6 and NFS7 were analyzed by obtaining electron backscatter diffraction patterns using the electron backscatter diffraction HKL Nordlys II detector with CHANNEL 5 software (details in Schmidt and Olesen, 1989) on the LEO 1450VP Scanning Electron Microscope at Bowdoin College. H7, H8, and H12 were analyzed using an EDAX-TSL-EBSD detector with TSL-OIM Data Collection software on the VEGA-XMU Scanning Electron Microscope at the University of Maine. The sections were oriented within the sample chamber at a 70° tilt and operating parameters during data collection included a chamber pressure of 10–15 Pa, an accelerating voltage of 15–20 kV, a working distance of 25 mm, and a probe current of ~2 nA. Acquisitions and indexing were typically set at 4 × 4 binning, high gain, a Hough resolution of 75, 7 bands, and 80 reflectors for the HKL-Channel 5 software and at 2 × 2 binning, high gain, a binned pattern size of 160, a theta step size of 0.5°, 8 bands, and 10 reflector families for the TSL-OIM software.

Quartz c-axis pole figures were obtained through the manual collection of indexed points or from automated quartz orientation maps of selected areas of foliation-parallel quartz veins. Automated maps were run at a step size at or greater than the diameter of the new quartz grain sizes (between 10 and 30 μm). The number and area of sampled quartz veins varied from section to section depending on the dimensions of the vein(s), the indexing percentage of each section, and the number of data points. Pole figures were created and contoured using both the Mambo module of the HKL Channel 5 software and the TSL-OIM software.

Our observations to date suggest that these veins record very high strains leading to δ angles $\leq 9°$. Five representative pole figures are shown in Fig. 5, including the sample with the highest

measured δ (NFS 6). These small δ angles are consistent with pole figures published by Hubbard and Wang (1999) from nearby mylonites and confirm that very high strains have accumulated on the SCMZ and other mylonitic strands of the NFS.

5.2. Method 1: oblique quartz SPO

Two measurements are necessary to determine β (Fig. 1) in a given sample: the angle λ_{ISA} between the foliation and the direction of elongation of new quartz grains (Fig. 2a), and the angle δ between the foliation and the normal to the quartz *c*-axis girdle (Fig. 2b). Wallis (1995) suggested that when measuring λ_{ISA}, the maximum measurement be taken as the value most closely representing the orientation of ISA_1. However, in practice we found a considerable range of quartz elongation directions owing presumably to (a) variations in the amount of strain accumulated by the measured grains after they formed and (b) local fabric rotations relative to the far-field ISA caused by mechanical heterogeneity (e.g., the presence of a feldspar porphyroclast just out of the section plane). We suggest that more robust estimates of W_m can be acquired by using numerous measurements of λ_{ISA} in each sample, adding an appropriate average correction for the δ angle measured from the c-axis pole figure, and calculating the mean value and standard deviation of the results to provide a range of W_m estimates.

When W_m has a value between 0.9 and 1.0, adding $\delta = 5^\circ$ would have a maximum effect on W_m of $0.02 \leq \Delta W_m \leq 0.06$. Given that (a) this range overlaps what we consider to be the typical range of error for the method and (b) the angle is estimated manually by drawing a line connecting c-axis maxima across the foliation plane, we settled on an approach whereby we added a δ angle of 5° to all of our measurements of λ_{ISA} rather than correcting each sample individually.

Fig. 6 shows data for five samples from which we collected quartz c-axis pole figures (Fig. 5). Following the methodologies described above, the results using Method 1 consistently indicate $W_m \geq 0.94$, and an average of these five samples gives $W_m = 0.97 \pm 0.03$.

5.3. Method 2: rigid clast rotation

Passchier (1987) introduced five criteria for the analysis of clast SPO fabrics: (1) the sample accumulated high enough finite strain so that clasts with appropriate shape factor could rotate to near-stable positions; (2) the fabric indicates reasonably homogeneous deformation on the scale of the sample; (3) the matrix grain size is much smaller than that of clasts; (4) clasts have regular shape and may be approximated by orthorhombic (or ellipsoidal) symmetry; and (5) clasts show a wide range of shape factors and are spatially well dispersed. SCMZ samples appeared to meet these core requirements reasonably well, so our aim was to collect enough clast measurements to differentiate between clasts that had assumed stable orientations and those that had rotated forward continuously in the flow.

For each sample, sets of photomicrographs were taken across entire large (5×7.6 cm) thin sections. The outlines of clasts were hand drawn in *ImageJ* (http://rsbweb.nih.gov/ij/), and the best-fit ellipse algorithm assigned a major (m_1) and minor (m_2) axis and orientation (θ) to each clast (Fig. 3a). From this, we calculated both axial ratio (R) and the cross-sectional shape factor (B). In choosing porphyroclasts for measurement, we attempted to minimize the effects of clast interaction by selecting isolated porphyroclasts where possible, and in regions with abundant clasts we selected mainly those with neighbors no closer than approximately twice their long radii. Clast interaction probably introduced some noise into our data, but given our methodology it is unlikely to have markedly affected the overall SPO fabric. Following Ghosh and Ramberg's (1976) theory of particle rotation and Passchier's (1987) criteria, W_m was estimated from the shape factor 'cut-off' between clasts that had apparently reached a stable orientation (higher B) and those that rotated continuously (lower B).

Fig. 7 plots the cross-sectional shapes and orientations of feldspar porphyroclasts for six samples (including those used for Figs. 5 and 6), and Fig. 8 shows photomicrographs of the same samples. Quartz volumes with well-developed SPO were not present in sample W63 precluding application of Method 1, but the spectacular feldspar and muscovite fish in this sample made it useful for clast analysis. The distribution of round clasts ($0 < B < 0.5$–0.6) in the samples is scattered but approximately symmetric about the foliation, consistent with the theoretical prediction that they rotated forward continuously without finding a stable orientation in the flow. In contrast, the distribution of elongate clasts (0.5–$0.6 < B < 1$) is asymmetric about the foliation, strongly clustering at small to intermediate positive θ values, consistent with these clasts approaching or having reached a stable orientation in the flow. In addition to feldspar clasts, Fig. 7g plots the cross-sectional shapes and orientations of mica fish in samples W63 and NFS7. Elongate feldspar porphyroclasts in these two samples cluster at unusually high θ values and overlap with the mica-fish data. This important observation will be discussed below.

5.4. Results and discussion

Table 1 shows ranges of W_m estimates made using Methods 1 and 2. Values range from 0.45 to 1.0 depending on the sample, method applied, and uncertainties associated with each method. It appears that either method gives internally consistent results, but results from one method differ markedly in comparison to the other. The relatively low estimate of W_m from Method 2 in comparison to other methods from the same rocks is common among studies that have utilized the clast method in combination with other methods (e.g., Wallis, 1995; Bailey and Eyster, 2003; Law et al., 2004; Jessup et al., 2006; Xypolias and Kokkalas, 2006). A number of explanations for this discrepancy are plausible, but we consider the following three explanations worthy of consideration.

(1) Method 1 can only access the last instant of deformation, having a shorter 'strain memory' than Method 2, so each method may be recording a different strain history. This explanation is conceivable but would require non steady-state deformation during which the angle α between the flow apophyses (Fig. 1) changed markedly near the end of the deformation history allowing Method 1 to record a much higher W_m than Method 2. It is difficult to discount this possibility conclusively, but we have no other evidence to support it.

(2) If quartz is markedly weak relative to the bulk mylonitic rock, then the quartz volumes used in Method 1 may represent zones of strain localization and vorticity partitioning, giving higher W_m values than expected for the bulk shear zone. To obtain the data in Fig. 6, we made numerous measurements of recrystallized quartz SPO across individual thin sections within a variety of discontinuous quartz volumes. Some of these volumes comprised just a few recrystallized quartz grains, whereas others comprised thin, discontinuous, foliation-parallel veins a few tens of grains in width (Fig. 2). If quartz was flowing under markedly lower differential stress than the surrounding matrix, then we would expect the wider, longer, foliation-parallel veins to show the largest λ_{ISA} and consequently the largest W_m.

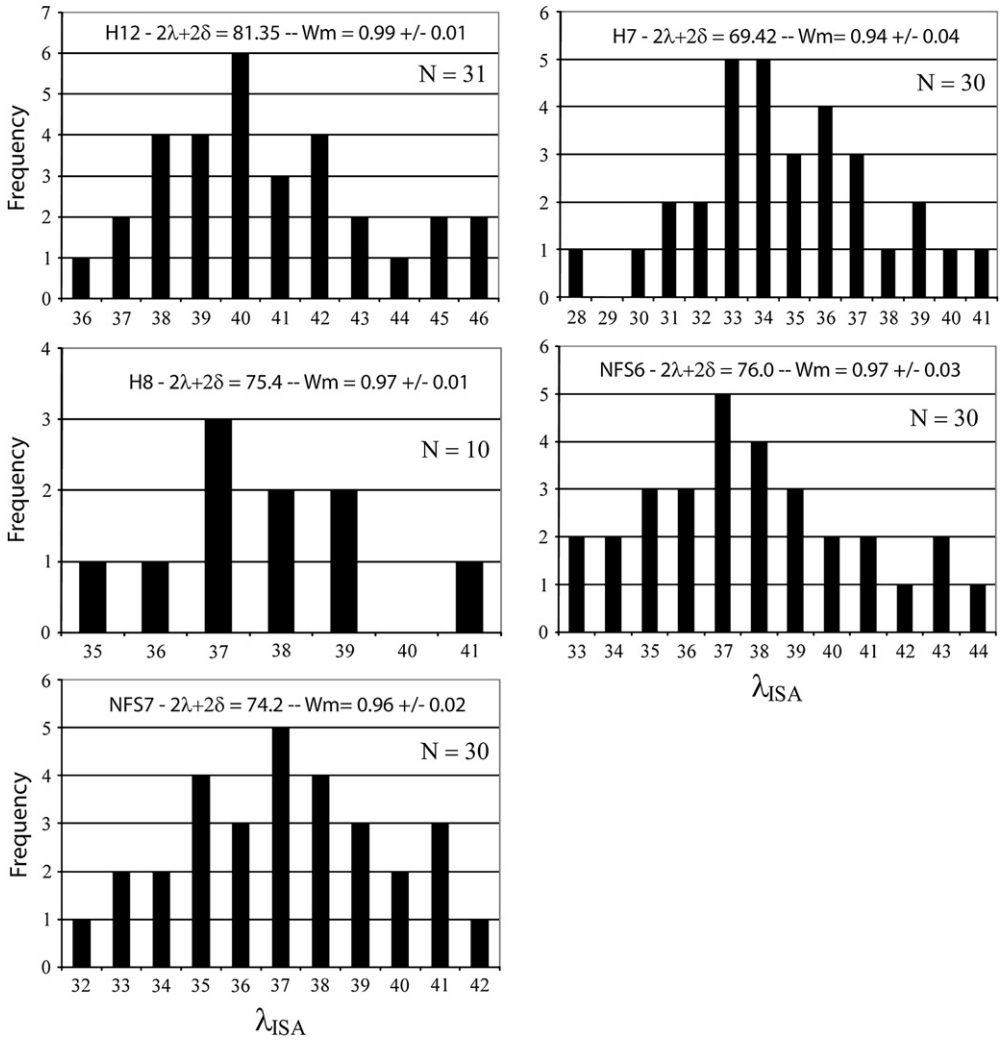

Fig. 6. Results of W_m estimates for the five samples shown in Fig. 5 using Method 1 – quartz oblique SPO. Estimates were acquired by making numerous measurements of λ_{ISA} in each sample, adding a 5° correction for the average δ angle, and calculating the mean value and standard deviation of the results. An average of these five samples gives $W_m = 0.97 \pm 0.03$.

However, a systematic relationship between polycrystalline quartz volume, morphology and W_m did not arise. One possible explanation for this is that the quartz and surrounding matrix may have had similar flow strengths under the prevailing deformation conditions. Alternatively, the discontinuous nature of the quartz volumes may have limited the partitioning of W_m to a relatively narrow range around the bulk matrix W_m. Given the lack of evidence for quartz flowing more readily than the surrounding matrix, we conclude that the creep strength of quartz relative to the surrounding matrix was not a critical contributor to the difference in results between Methods 1 and 2, although it may be responsible for some of the variance in our data (Fig. 6).

(3) Conditions in the SCMZ rocks may violate fundamental assumptions regarding clast interaction or clast/matrix coupling necessary for the application of Method 2. This explanation invites the following considerations.

Consideration 1: A major precondition for using Method 2 to estimate W_m is that clasts rotated as solitary, isolated objects in a viscous rock matrix. However, natural samples, including those from the SCMZ, typically contain many clasts per thin section, and the interaction of these clasts can affect their rotational behavior and surrounding flow patterns (Ildefonse et al., 1992a,b; Piazolo et al., 2002; Samanta et al., 2003). The likelihood of clast interaction affecting the clast SPO is highest in those areas where new clasts were created by fracturing and fragmentation of parent clasts near the end of the deformation history. Our criterion of selecting relatively isolated, whole, rounded clasts for analysis helped to minimize the effects of clast interaction on SPO fabric strength. Given the care that we used in selecting clasts for measurement, we discard clast interaction as a critical contributor to the difference in results between Methods 1 and 2, although it is probably responsible for some of the variance in our data (Fig. 7).

Consideration 2: A second major precondition for using Method 2 to estimate W_m is that perfect Newtonian viscous coupling occurred between clasts and a single-viscosity rock matrix. As reviewed in the *Introduction* above, analog and numerical models show that strain localization arising from a thin low-viscosity layer or other slip condition at the surfaces of rigid clasts in slow viscous flows can markedly affect their rotational behavior, so the reliability of clast SPO as an indicator of W_m may be compromised by such localization. We suggest that this is the primary cause of the discrepancy between Methods 1 and 2 shown in Table 1 and we use

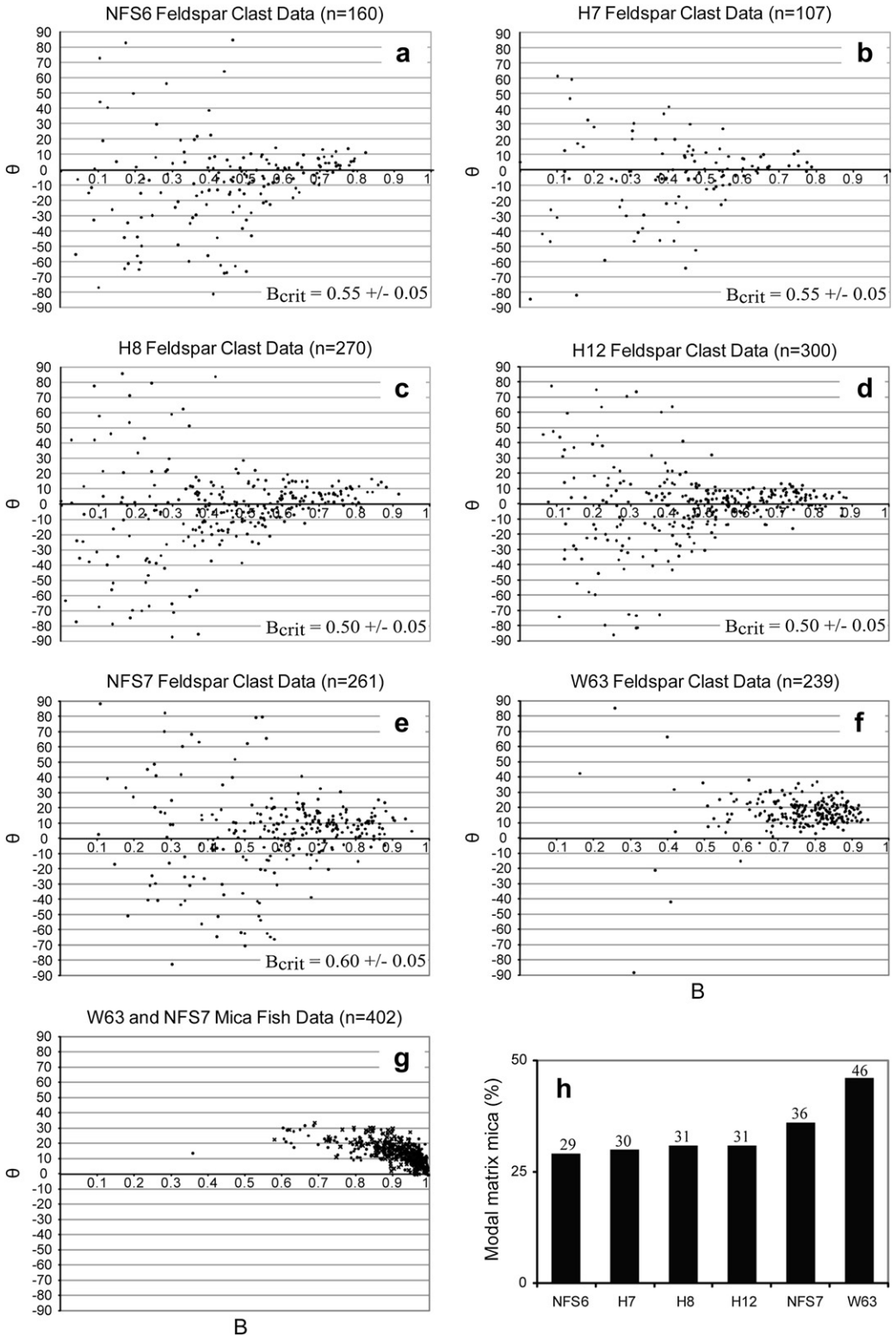

Fig. 7. Shape preferred orientation data for feldspar clasts and mica fish and modal matrix mica in rocks from the SCMZ. The angle θ in (a)–(g) is the measured angle between the long axis of a clast or mica fish and the mylonitic foliation. The shape factor B is defined in the text. The approximate position of B_{crit} is indicated for all feldspar clast data with the exception of sample W63, which is indeterminate owing to lack of clasts with $B < B_{crit}$. Modal matrix mica content in (h) shows similar percentages for NFS6, H7, H8 and H12, with mica mode increasing through NFS7 to W63 where it comprises 46% of the matrix. The increase in modal matrix mica correlates to the increased θ of feldspar clasts in NFS7 and W63. Mica fish were not included when calculating the modal matrix mica.

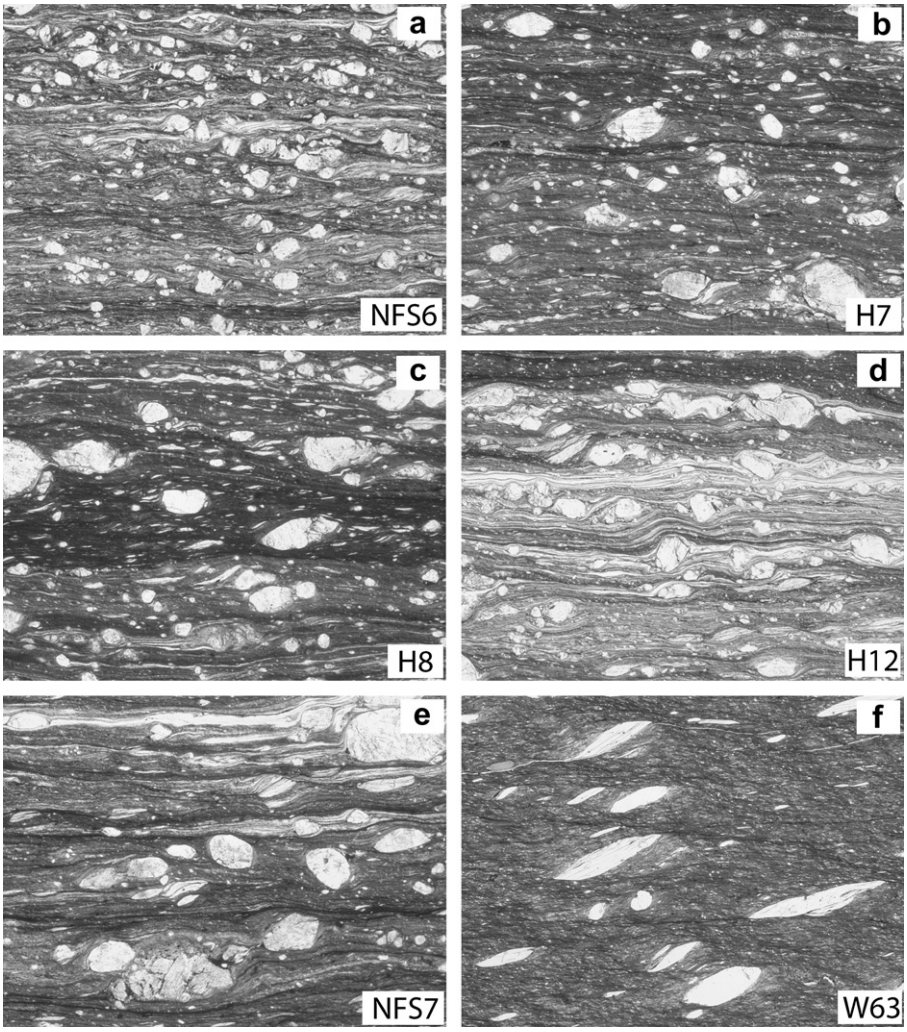

Fig. 8. Photomicrographs of the thin sections from which the data in Fig. 7 were collected. For all photomicrographs: plane polarized light, dextral shear sense, lineation-parallel section, long axis 5.9 mm.

numerical models to explore this phenomenon in the following section.

The distribution of elongate feldspar clasts ($B > B_{crit}$) is asymmetric about the foliation in all six samples, strongly clustering at positive θ values. Theoretically, if there is perfect coupling between the clasts and a single-viscosity Newtonian matrix, with no strain localization or slip at the clast interfaces, the distribution of elongate clasts ($B > B_{crit}$) should be asymmetric about the foliation and strongly clustered at small *negative* θ values for dextral shear. We can illustrate this by rearranging the clast data for sample H12 in Fig. 7 to develop the hypothetical distribution shown in Fig. 9. If the cutoff value of $B = 0.50$ were valid, then the clast data should cluster along the theoretical curve from Ghosh and Ramberg (1976)

Table 1
Comparison of W_m estimates made using Methods 1 and 2.

Sample	W_m – Method 1	W_m – Method 2
H7	0.94 ± 0.04	0.55 ± 0.5
H8	0.97 ± 0.01	0.50 ± 0.5
H12	0.99 ± 0.01	0.50 ± 0.5
NFS6	0.97 ± 0.03	0.55 ± 0.5
NFS7	0.96 ± 0.02	0.60 ± 0.5

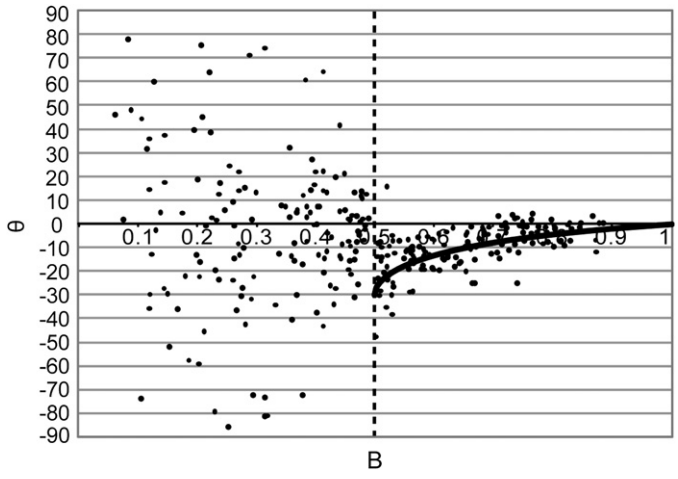

Fig. 9. Hypothetical orientation distribution for the 300 clasts of sample H12. Actual θ values are offset by a linear function of B to fit the solid black curve that indicates the theoretical stable position for $W_k = 0.5$ using Eq. (8). The curve ends at $B_{crit} = 0.5$ as indicated by the vertical dashed line.

for $W_k = 0.50$ (Eq. (8)), as shown in Fig. 9. The elongate clasts in sample H12 fall well away from this theoretically predicted distribution, as do the data from all of our samples. We note that adding the δ angle (5°) from the quartz c-axis data to the θ value for each clast would increase the deviation from the predicted distribution.

An important observation is that the amplitude of elongate clast SPOs increases in samples NFS7 and W63 relative to the other samples (Fig. 7). While investigating possible explanations for this trend, we discovered that modal matrix mica content increases in these two samples relative to the others (Fig. 7h). This relation between clast SPO amplitude and modal matrix mica content leads to the hypothesis that mica facilitates localization at the clast/matrix interface. If so, then we surmise that mica fish should be self-lubricating and would form an end-member SPO, regardless of matrix modal mica content. As part of our analysis, we collected measurements on mica fish shapes and orientations in samples NFS7 and W63 (Fig. 7g). Remarkably, feldspar clast SPOs trend progressively towards the mica fish SPO with increasing matrix mica content, and the feldspar clast SPO in sample W63 strongly overlaps with the mica fish SPO. An important addition to our observation is that mica fish in very pure quartzite mylonites (Lister and Snoke, 1984; ten Grotenhuis et al., 2002, 2003) show similar SPO to our own data (Fig. 10). For example, Fig. 10b shows mica fish data from ten Grotenhuis et al. (2002, fig. 2). Because these mylonites are very quartz-rich, it would appear in these instances that the mica fish are self-lubricating, which may be facilitated by very thin, fine-grained recrystallization or reaction rims at the fish/matrix interfaces. These important observations add support our supposition that mica plays a crucial role in clast lubrication, and we will explore this more fully in the following section where we show that the mica-fish data are bounded by a numerical relation that suggests total slip at their interfaces.

6. Numerical models

In this section we use numerical models to explore how the rotational behavior of isolated clasts changes when strain localizes at their margins and whether such changes can explain the clustering in positive θ of clasts with $B > B_{crit}$. Building on previously published models that explore object lubrication (e.g., Marques et al., 2005a,b; Schmid and Podladchikov, 2005; Johnson, 2008), we add the kinematic vorticity number as a parameter and conduct sensitivity analyses across the range $0 < W_k \leq 1$.

We employ the finite element method using Comsol Multiphysics software (http://www.comsol.com/) to deform a 2-D fluid 'shear box'. Fixed velocity boundary conditions (Fig. 11) define the strain rate and vorticity within the region with choice end members of flow ranging from pure shear ($W_k = 0$) to simple shear ($W_k = 1$); supersimple shear ($W_k > 1$) is not considered in this study. The flow field is perturbed by an elastic elliptical clast located at the center of the shear box and enveloped by a thin layer, the viscosity of which can be varied relative to the surrounding linear viscous matrix. A triangular (advancing front) mesh was used, and a typical model had in excess of 5000 elements with the highest element concentration at the clast boundaries (Fig. 11).

For each model, we specify the clast shape (B), initial orientation (θ), and the viscosity ratio (η) defined as the ratio between the matrix viscosity and the enveloping-layer viscosity. In all models, additional variables are held constant at the following values: (1) the matrix viscosity is 10^{18} Pa s, (2) the Young's modulus of the clast is 2×10^{14} Pa, and (3) the clast's long diameter is fixed at 10% of the shear box width in order to minimize the effects of confined flow on clast rotation (e.g., Bons et al., 1997; Biermeier et al., 2001; Marques et al., 2005a). Most of our analyses were carried out using an enveloping-layer thickness (H) that is 5% of the clast radius.

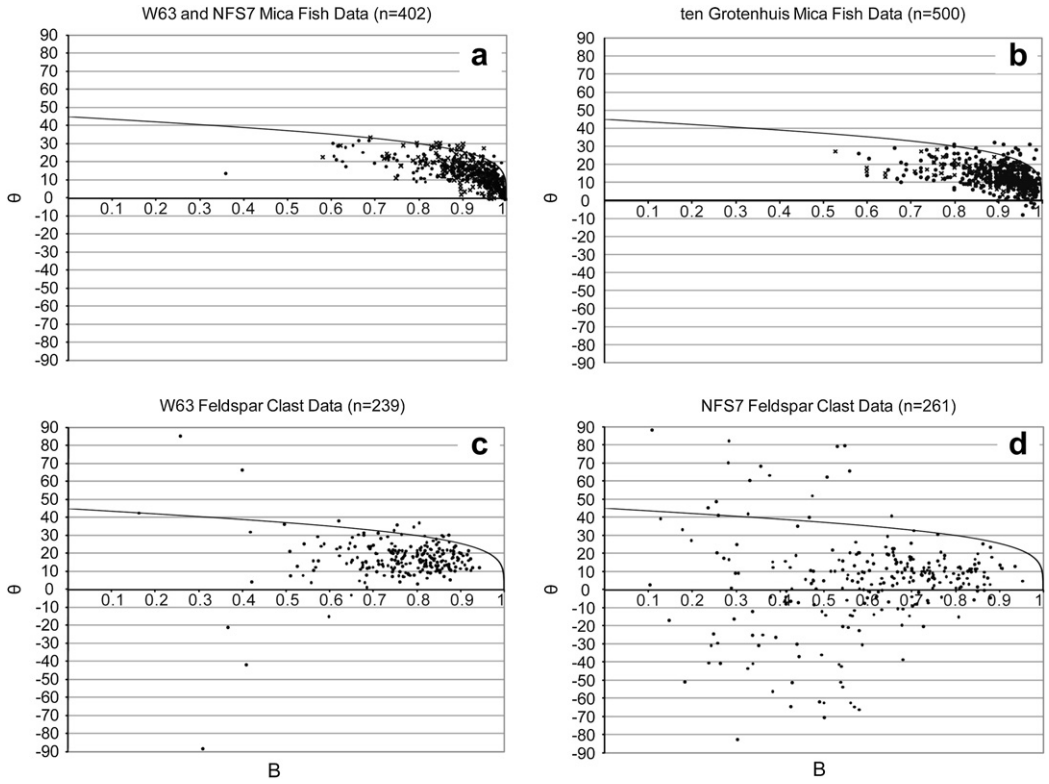

Fig. 10. Shape preferred orientation data for mica fish from samples NFS7 (dots, $n = 228$) and W63 (crosses, $n = 174$), and from the California (crosses, $n = 100$) and Brazil (dots, $n = 400$) localities of ten Grotenhuis et al. (2002, fig. 2a). For comparison, feldspar data are also shown for NFS7 and W63. Note that the SPOs of feldspar clasts trend towards the mica fish SPO with increasing modal matrix mica (Fig. 7h). The curve is for total slip at the matrix/clast interface for $W_k = 1.0$ (Mulchrone, 2007).

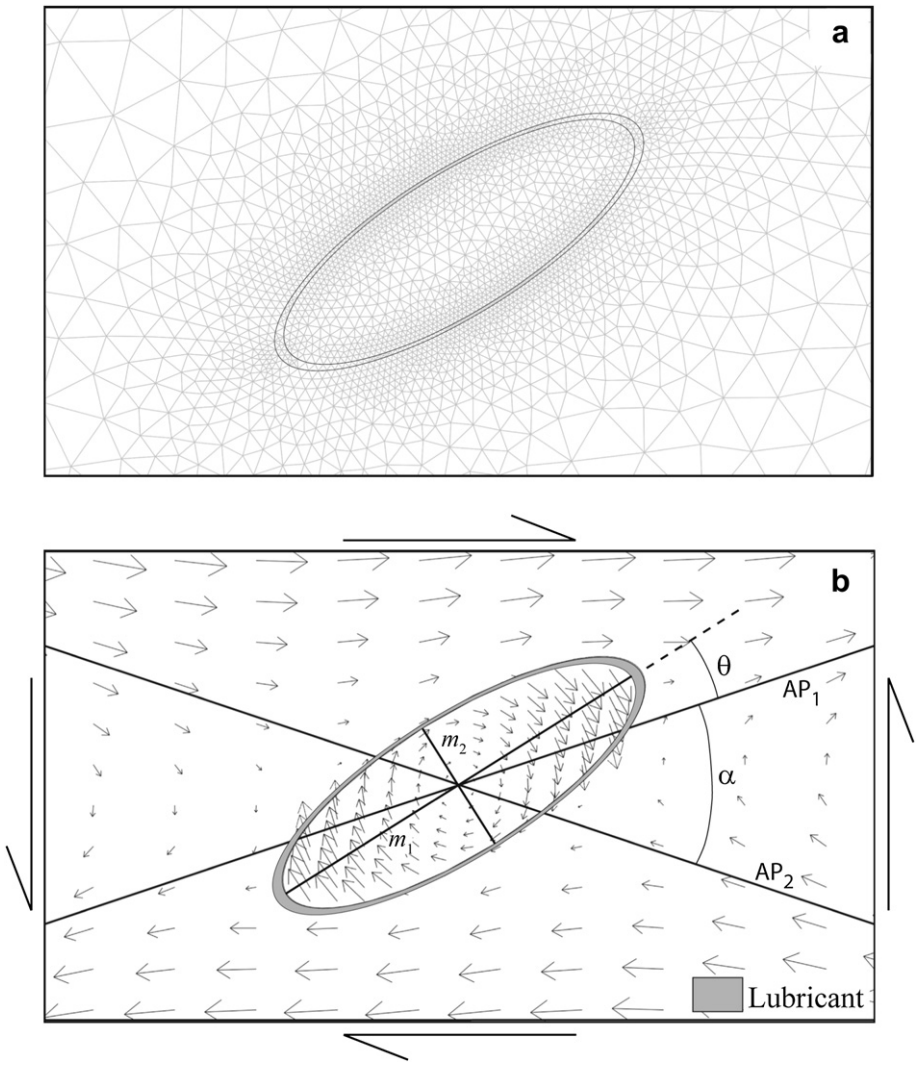

Fig. 11. Details of the numerical matrix/clast system. (a) Central portion of the finite element mesh illustrating the concentration of mesh elements at the clast boundaries. (b) Solution for model with $B = 0.8$, $W_k = 0.8$ and $\acute{\eta} = 16$. Constant-velocity boundary conditions are indicated by single-sided arrows on boundaries, with values depending on W_k. Considering the model scaling, the maximum far-field viscous shear strain rate is $10^{-14}\,s^{-1}$ for $W_k = 1.0$. Internal arrows indicate velocity relative to clast center with the clast rotating clockwise towards the stable position. AP_1 and AP_2 are far-field flow apophyses, and m_1 and m_2 are maximum and minimum clast diameters. The clast is effectively rigid compared to the viscous matrix. The thickness of the lubricating layer (shaded region) is 5% of the clast radius.

Schmid and Podladchikov (2005) have shown that clast stable positions are sensitive to H, particularly at relatively small viscosity contrasts. Although we did not conduct a detailed sensitivity analysis, we show results of selected model runs with $H = 10\%$ and 20% of the clast radius and illustrate how these results compare with solutions in which $H = 5\%$.

In conducting our sensitivity analyses, we initially tested clast shapes in increments of $B = 0.1$ and then strategically chose B values between these initial increments where necessary in order to establish continuous curves in $B - \theta$ space. Large deformation of the clast/lubricant/matrix system would lead to a time-dependent change in the parameter H. In order to avoid this, we iteratively rotated each undeformed clast and enveloping layer into a new position, applied a small strain, and examined the clast's angular velocity. We proceeded this way until we located the approximate orientation in which the clast rotation reversed direction. Once we identified this orientation, we reduced the rotation increments and determined stable positions (zero angular velocity) to within $\pm 0.25^\circ$.

Fig. 12 shows the results of our models. Each solution shows a 'family' of SPO curves representing the stable orientations θ_s of clasts as a function of B for various W_k values and a fixed viscosity contrast $\acute{\eta}$. In Fig. 12a, the points represent numerical results, and the curves are from the analytical solution of Ghosh and Ramberg (1976), calculated from Eq. (8). These results provide analytical validation of our numerical methodology. In Fig. 12b–d, the points represent numerical solutions, and the curves are best fits to those points. Perfectly coupled clasts ($\acute{\eta} = 1$, Fig. 12a) exhibit SPO curves that are reclined ($\theta_s < 0$) with respect to a foliation fixed to the extensional flow apophysis (AP_1) for all B. A comparison between Fig. 12a and the data in Fig. 7 clearly shows a departure of presumably stable clast orientations ($B > B_{crit}$) from those predicted for a rigid object in a single-phase Newtonian matrix. Lubricated clasts (*e.g.*, $\acute{\eta} = 16$, 64 and 1024; Fig. 12b–d) exhibit SPO curves consisting of both reclined portions ($\theta_s < 0$) and inclined portions ($\theta_s > 0$). The reclined portion of each SPO curve terminates at a characteristic point on the 'B_{crit} envelope' of its family (dotted lines in Fig. 12a–d). Note that the inclined portions increase in amplitude with increasing W_k. In addition, the termination point for each W_k curve on its B_{crit} envelope moves to lower B values with increasing viscosity contrast. The termination point of a W_k curve on the B_{crit} envelope defines the SPO cutoff traditionally used to determine W_m from clast populations. This cutoff is highly sensitive

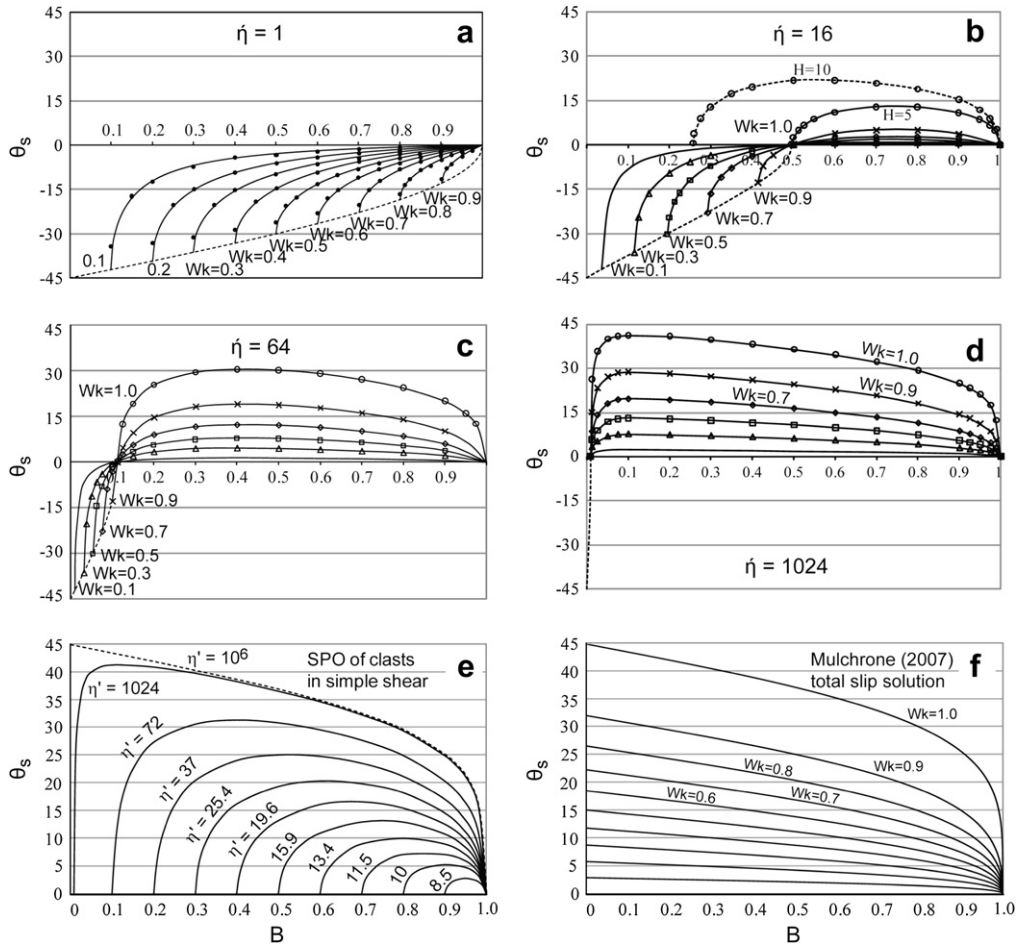

Fig. 12. Curves showing the shape preferred orientations of *stable* clasts as a function of W_k, B and $\dot{\eta}$. (a) Validation experiment showing that our numerical data (dots) match the analytical solutions (curves) of Ghosh and Ramberg (1976). (b), (c) and (d) Numerical results with best-fit curves showing how the stable clast positions are expected to change with increasing lubrication at the matrix/clast interface for $\acute{\eta} = 16$, 64 and 1024. For $\acute{\eta} = 16$, we show the effect of increasing H to 10% for $W_k = 1$. (e) Family of curves for $W_k = 1.0$ showing the $\acute{\eta}$ values required to cross $\theta = 0$ across a range of B values (H = 5% in all cases). The dashed curve approximates the total slip condition, with $\acute{\eta} = 10^6$. (f) Analytical solution for total slip across Wk values 0.1 to 1.0 (Mulchrone, 2007). The analytical curve for $W_k = 1.0$ and our numerical solution for $W_k = 1.0$ and $\acute{\eta} = 10^6$ are approximately identical.

to the degree of matrix/clast coupling. For example, the B_{crit} termination for $W_k = 0.9$ changes from $B = 0.9$ to ~0.4 to ~0.1 for $\acute{\eta} = 1$, 16 and 64, respectively. The cutoff is also highly sensitive to H. Fig. 12b shows the difference for $H = 5\%$ and $H = 10\%$ of the clast radius for $\dot{\eta} = 16$ and $W_k = 1.0$. In this example, the B_{crit} termination changes from $B = 0.5$ to ~0.25.

Our numerical results show that the cutoff value shifts towards smaller B values with increasing $\dot{\eta}$ and H. This means that rigid clast methods for determining W_m, as currently applied, are unreliable in the absence of a perfect (or well-known) coupling and a known lubrication layer thickness. Our results provide an elegant explanation for why these methods typically underestimate W_m relative to other methods (e.g., Wallis, 1995; Bailey and Eyster, 2003; Law et al., 2004; Sullivan, 2008). In addition, our analysis shows that the amplitude (θ) of the inclined portion of the clast data distribution is sensitive to W_k, particularly for W_k values near 1.0. θ is also sensitive to H, particularly at relatively low $\acute{\eta}$ values, as shown by Schmid and Podladchikov (2005). For sample H12, given the cutoff at $B = 0.50 \pm 0.05$ and the maximum amplitude of $\theta \approx 10^\circ$, only curves with $H \approx 5\%$ and $W_k \approx 1.0$ can bound the data with $\acute{\eta} \approx 16$ (compare the amplitude of clast data in Fig. 7d with curve amplitudes in Fig. 12b). If we consider $H = 10\%$, then the data could be bound using a lower $\acute{\eta}$ value, but the data amplitude would still require a high W_k value approaching 1.0. Thus, clast data may still be useful for estimating W_m, but in practice the data may only be useful for indicating whether or not W_m is near 1.0 because of the large amplitude difference between curves for $W_m \approx 1.0$ and curves for $W_m \leq 0.9$. Given the apparent importance of the amplitude of the data distribution for constraining W_m, H and $\acute{\eta}$, the angle between the clast long axis and foliation should also be corrected where possible by adding the δ angle from quartz c-axis pole figures (Fig. 2). Using the same reasoning applied above for sample H12, all of the feldspar clast data in Fig. 7 (with the exception of sample W63, which is indeterminate owing to the lack of low-B clasts) would suggest that W_m is near 1.0, consistent with the results obtained from the oblique quartz SPO technique (Table 1). This raises the interesting proposition that the oblique quartz SPO technique provides useful estimates of W_m in rocks where the rigid clast rotation technique is compromised by clast lubrication. However, the possibility that W_m obtained from quartz-rich volumes may not be representative of W_m for the bulk shear zone must be considered, as discussed above.

As a summary plot, Fig. 12e shows that the SPO of clasts in simple shear ($W_k = 1.0$) can be represented as a function of B for various $\acute{\eta}$ values (note that $H = 5\%$ in all of these curves). As $\acute{\eta}$ approaches infinity, these curves approach a total slip condition approximated in our numerical models by $\acute{\eta} = 10^6$ (dashed line in Fig. 12e). Like the inclined portions of SPO curves in Fig. 12b–d, the total slip envelope should vary in amplitude with W_k. In fact, this has been shown analytically by Mulchrone (2007), and in Fig. 12f

we show his solutions for $W_k = 0.1$ to 1.0. Mulchrone's (2007) total slip solution for $W_k = 1.0$ is effectively identical to our numerical solution for $W_k = 1.0$ and $\acute{\eta} = 10^6$, providing additional validation for our numerical results. As shown by Schmid and Podladchikov (2005), solutions at very high $\acute{\eta}$ are not sensitive to H. Thus, our total slip approximation and Mulchrone's (2007) total slip solutions are independent of H.

Mulchrone's (2007) total slip curve for $W_k = 1.0$ is shown in Fig. 10, where it forms a tight bound on mica fish SPO from both the SCMZ and data from ten Grotenhuis et al. (2002). Fig. 10 also shows the SPO of feldspar clasts in samples NFS7 and W63, where a trend towards the mica fish SPO with increasing modal mica content is apparent (W63 has higher modal matrix mica than NFS7, as shown in Fig. 7h). This is an important result because it shows that the SPO of lubricated clasts is a function of interface coupling and that mica fish form an end-member owing presumably to their extremely weak interfaces. Thus, mica-rich rocks show greater clast lubrication, consistent with mica playing the key role in lubrication. The bound on our clast data in Fig. 10 is additional evidence that W_m is near 1.0 in these rocks, as suggested by Method 1 (Table 1), and that the relatively low B_{crit} values in Fig. 7 are caused by clast lubrication and do not accurately reflect W_m.

An interesting result from our analysis is that all W_k curves for a particular $\acute{\eta}$ family cross the $\theta_s = 0$ axis at the same B value (Fig. 12). This allows us to define a characteristic shape factor B^* that stably aligns parallel to AP_1 for a given $\acute{\eta}$ and that is independent of W_k. This result leads to Fig. 13, which plots the characteristic shape factor B^* against both $\acute{\eta}$ and $1/\acute{\eta}$ for $H = 5$, 10 and 20% of the clast radius. If B^* can be determined through plotting an appropriately large number of clast measurements and if an average H value can be obtained, then the approximate viscosity contrast can be determined from Fig. 13 without knowledge of W_m. For example, in H12 and NFS7 the B cutoff values might be taken as ca. 0.50 and 0.60, respectively, leading to $\acute{\eta} \approx 15.9$ and 13.4 for $H = 5\%$. If mica is the key lubricating phase, then this opens the possibility of assigning a strength, or relative viscosity, to the matrix through the definition of $\acute{\eta}$ and the use of existing flow laws for mica (e.g., Kronenberg et al., 1990). Unfortunately, the sensitivity of the $\acute{\eta} - B^*$ relation to H adds considerable uncertainty to such an analysis (Fig. 13), and it will probably remain a qualitative tool only.

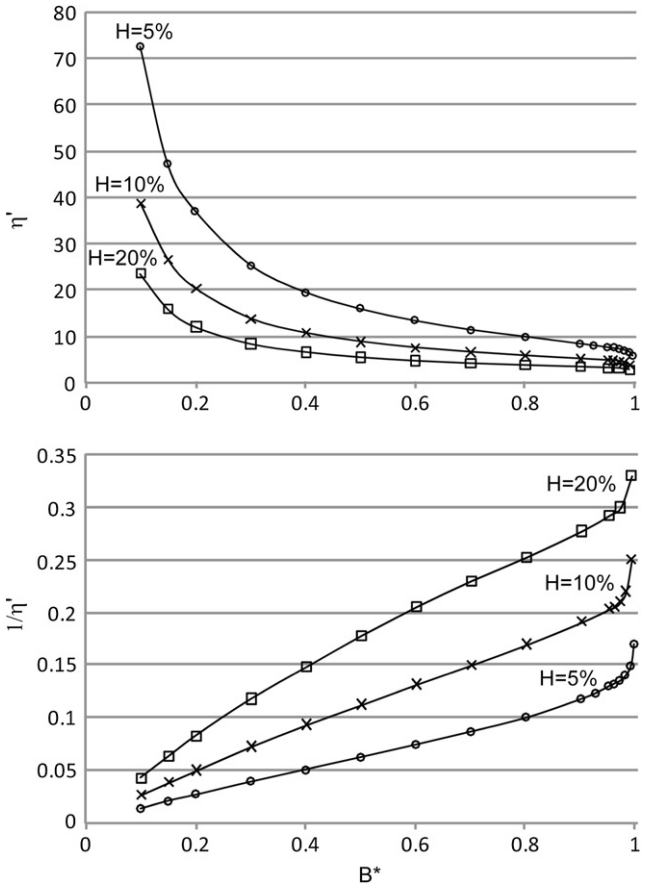

Fig. 13. Plots showing the relationship between the characteristic shape factor B^* and (a) $\acute{\eta}$ or (b) $1/\acute{\eta}$. Three different H values are plotted in each. In theory, determining the characteristic cutoff B^* and an average H value could allow for the determination of $\acute{\eta}$ without knowledge of W_m. Note that the relation between B^* and $1/\acute{\eta}$ is approximately linear for $B^* < 0.95$.

7. Discussion and conclusions

(1) Our data and numerical models show that the critical shape factor cutoff B_{crit} separating clasts in stable positions from those rotating continuously is highly sensitive to the degree of clast/matrix coupling. Where strain localization occurs at the clast margins, the value of B_{crit} is reduced, leading to erroneous estimates of W_m. This provides a robust explanation for the fact that clast methods commonly give lower estimates of W_m when compared to other methods in the same rocks. Several papers have noted a wide range of W_m estimates when using a clast method in comparison to other methods (e.g., Wallis, 1995; Bailey and Eyster, 2003; Law et al., 2004; Jessup et al., 2006; Xypolias and Kokkalas, 2006; Sullivan, 2008). Large variations in W_m estimates demand the consideration of either non-steady flow (leading to variation of W_m through time), or spatial partitioning of W_m (owing to rheological variation or proximity to a major structure). Alternatively, if estimates are based on W_m values derived from clast methods, then the possiblity that clast lubrication has rendered the W_m unreliable should be evaluated.

(2) In our study, the amplitude (θ value) of clast SPO for $B > B_{crit}$ is a function of both W_k and, apparently, the degree of strain localization at the clast margin. Four observations suggest to us that mica plays a key role in clast lubrication in our samples. (a) The progressive trend of feldspar SPOs towards the mica fish position in samples NFS7 and W63 corresponds with a marked increase in modal matrix mica content. (b) Thin mica-rich rims are commonly observed surrounding feldspar clasts in our samples and in others (e.g., Schmid and Podladchikov, 2005), and are best developed in those samples with greater modal matrix mica (Fig. 14). (c) Pennacchioni et al. (2001) also documented sillimanite, plagioclase and garnet grains in stable positions indicative of clast lubrication in mylonites with very high modal matrix biotite. (d) Mica fish can occur in very pure quartzite mylonites (Lister and Snoke, 1984; ten Grotenhuis et al., 2003), where it is possible that they are self-lubricating. Mica is known to be one of the weakest minerals in shear along its {001} planes at greenschist to lower amphibolites facies conditions, consistent with mylonite development (e.g., Kronenberg et al., 1990; Niemeijer and Spiers, 2005; Mariani et al., 2006). Alternatively, the presence of mica is known to dramatically affect the rates of diffusion (e.g., Farver and Yund, 1999) and dissolution–precipitation processes at wet interfaces between micas and other minerals (e.g., Niemeijer and Spiers, 2005; Meyer et al., 2006). Thus, the clast or mica fish interfaces may be weak owing to slip along mica {001} faces and/or enhanced dissolution–precipitation rates.

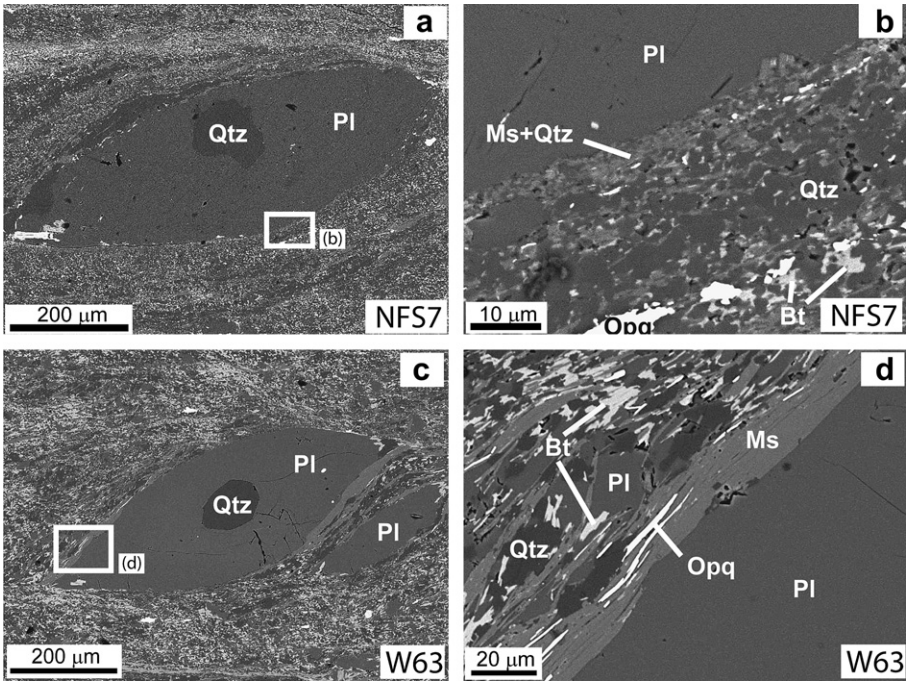

Fig. 14. Electron backscatter images of the boundaries of two plagioclase porphyroclasts from samples NFS7 (a, b) and W63 (c, d). A narrow rim rich in muscovite but also containing quartz occurs around the clast in (b), whereas the clast margin in (d) has a rim of effectively pure muscovite. Note that the nature of the rims varies around any single clast, but in general we have observed more mica-rich rims in NFS7 and W63 than in the other samples. Pl = plagioclase, Qtz = quartz, Ms = muscovite, Bt = biotite, Opq = Fe–Ti oxide.

(3) It may appear contradictory that increasing modal matrix mica correlates with increasing θ because increasing the modal mica would generally be expected to reduce the shear strength of the matrix, which, for homogeneous matrix deformation, would reduce $\acute{\eta}$ and therefore θ values for $B > B_{crit}$. One possible explanation is that increasing modal matrix mica violates the requirement of homogeneous matrix deformation by promoting the development of discrete zones of strain partitioning which has been shown to result in positive θ values for $B > B_{crit}$ (ten Grotenhuis et al., 2002). An equally plausible explanation is that increasing modal matrix mica enhances the accumulation of mica around clast margins, particularly if dissolution of matrix quartz and feldspar at clast margins is an active mechanism of mica concentration, thus achieving more complete lubrication. Given the data and the results of previous studies, it seems reasonable to suggest that in the higher modal matrix mica samples where feldspar clasts approach the mica fish position (samples NFS7 and W63, Fig. 10), the clast SPOs may result from a combination of strain localization into discrete matrix shear zones and locally near-complete clast/matrix decoupling through enhanced mica accumulation at clast margins.

(4) In our numerical models, and those of Schmid and Podladchikov (2005), the thickness of the lubricating layer (parameter H) was shown to have an important effect on clast kinematics. Among other plausible explanations, the variance in our natural data for $B > B_{crit}$ (Fig. 7) could reflect different H values for each clast. However, we wonder whether this parameter has real physical significance or whether it is simply a proxy in numerical models for other factors such as the percentage of a clast's surface in contact with mica, or some poorly understood physical/chemical processes related to atomic interactions across mineral interfaces (e.g., Meyer et al., 2006). It is also questionable whether completely surrounding a clast with a lubricating shell, as done here and by Schmid and Podladchikov (2005), is a reasonable description of the real rock. An alternative explored by Johnson (2008) is that mica "caps" that form on the foliation-parallel sides of clasts supply the lubrication, whereas the strain shadow sides of the clast are typically in contact with other minerals, such as quartz. Given that mica/feldspar interfaces behave differently from quartz/feldspar interfaces, the resulting relationships among B, W_m, $\acute{\eta}$, H and θ_s should be quite different from those presented here. Additional numerical models solving for both continuous and discontinuous contacts are required to address these questions. In addition, further microchemical and microphysical investigations are necessary for a more completely understanding of mineral interfaces and the factors that affect their interactions.

(5) Investigating whether or not a clast population has enjoyed lubrication requires a large data set with the appropriate dispersion in shape factor B. From our samples in Fig. 7, for example, the asymmetrical clustering of points for $B > B_{crit}$ is more convincing for H12 than it is for H7. In some published data sets (e.g., fig. 9 in Xypolias and Kokkalas, 2006), there are too few data at $B > B_{crit}$ to confidently evaluate the distribution. In other published data sets (e.g., fig. A1 in Jessup et al., 2006), many samples contain enough points at $B > B_{crit}$ to show asymmetry about $\theta = 0$. In addition, quartz c-axis pole figures are available for some of the data sets noted above, and some of these pole figures show δ values in excess of 10°. Adding these δ angles to the clast plots would significantly affect the distribution asymmetry.

(6) The geometry of mica fish and the mechanisms by which they form from larger precursor clasts have been well studied (e.g., Lister and Snoke, 1984; ten Grotenhuis et al., 2003). However, the primary cause of the characteristic mica fish orientation (e.g., Fig. 10) is not well understood.

Lister and Snoke (1984) and ten Grotenhuis et al. (2002, 2003) recognized that an orientation inclined to the flow was related to strain partitioning into narrow C-surfaces or shear bands, and ten Grotenhuis et al. (2002, 2003) noted that the stable orientation reflects a balance of forces around the object caused by flow separation. Adding to this knowledge, our results indicate that the mica fish orientation is effectively an end-member in lubricated clast geometry, with the data bounded by stable clast orientation envelopes that essentially indicate total lubrication of the fish margins. We suggest that this finding, and the changing feldspar clast orientations with increasing matrix modal mica (Fig. 10), reflects the "strength" of the crystalline interface between micas and other minerals.

(7) An important limitation of our numerical models is the assumption of Newtonian rheology. Introducing non-Newtonian rheology (e.g., Ildefonse and Mancktelow, 1993; Pennacchioni et al., 2000; Piazolo et al., 2002; Schmid and Podladchikov, 2005) will not change our overall conclusion that clast lubrication compromises the kinematic vorticity gauge, but details of the behavior and the possible effects on clast interaction (Ildefonse and Mancktelow, 1993; Piazolo et al., 2002) may be worthy of further investigation.

Acknowledgements

We gratefully acknowledge support from National Science Foundation grants EAR-0236756, EAR-0810039, EAR-0911150, CCLI-9951390, MRI-0320871 and MRI-0820946, a University of Maine Chase Distinguished Research Assistantship (NAP) and a University of Maine Doctoral Research Fellowship (JHM). Saskia ten Grotenhuis supplied the mica fish orientation data shown in Fig. 10b. Kieran Mulchrone provided a user-friendly equation for calculating the curves in Fig. 12f. We thank reviewers Albert Griera and Saskia ten Grotenhuis for thorough and constructive reviews that led to important improvements. Cees Passchier is thanks for his editorial guidance.

References

Arbaret, L., Mancktelow, N.S., Burg, J.P., 2001. Effect of shape and orientation on rigid particle rotation and matrix deformation in simple shear flow. Journal of Structural Geology 23, 113–125.

Bailey, C.M., Eyster, E.L., 2003. General shear deformation in the Pinaleno Mountains metamorphic core complex, Arizona. Journal of Structural Geology 25, 1883–1892.

Bailey, C.M., Francis, B.E., Fahrney, E.E., 2004. Strain and vorticity analysis of transpressional high-strain zones from the Virginia Piedmont, USA. Flow Processes in Faults and Shear Zones. In: Geological Society of London, Special Publications, vol. 224 249–264.

Bailey, C.M., Polvi, L.E., Forte, A.M., 2007. Pure shear dominated high-strain zones in basement terranes. Geological Society of America Memoir 200, 93–108.

Beam, E.C., Fisher, D.M., 1999. An estimate of kinematic vorticity from rotated elongate porphyroblasts. Journal of Structural Geology 21, 1553–1559.

Ben-Zion, Y., Sammis, C.G., 2003. Characterization of fault zones. Pure and Applied Geophysics 160, 677–715.

Bobyarchick, A.R., 1986. The eigenvalues of steady state flow in Mohr space. Tectonophysics 122, 35–51.

Bons, P.D., Barr, T.D., ten Brink, C.E., 1997. The development of delta-clasts in non-linear viscous materials: a numerical approach. Tectonophysics 270, 29–41.

Biermeier, C., Stúwe, K., Barr, T.D., 2001. The rotation rate of cylindrical objects during simple shear. Journal of Structural Geology 23, 765–776.

Carosi, R., Montomoli, C., Rubatto, D., Visonà, D., 2006. Extensional shear zones in the core of the Higher Himalayan Crystallines (Bhutan Himalayas): evidence for extrusion? In: Geological Society of London Special Publication, vol. 268 425–444.

Ceriani, S., Mancktelow, N.S., Pennacchioni, G., 2003. Analogue modelling of the influence of shape and particle/matrix interface lubrication on the rotational behaviour of rigid particles in simple shear. Journal of Structural Geology 25, 2005–2021.

Doll, W.E., Domoracki, W.J., Costain, J.K., Coruh, C., Ludman, A., Hopeck, J.T., 1996. Implications of a seismic reflection profile across a portion of the Norumbega fault system, east-central Maine. Geology 24, 251–254.

Farver, J.R., Yund, R.A., 1999. Oxygen bulk diffusion measurements and TEM characterization of a natural ultramylonite: implications for fluid transport in mica-bearing rocks. Journal of Metamorphic Geology 17, 669–683.

Forte, A.M., Bailey, C.M., 2007. Testing the utility of the porphyroclast hyperbolic distribution method of kinematic vorticity analysis. Journal of Structural Geology 29, 983–1001.

Fossen, H., Tikoff, B., 1998. Extended models of transpression and transtension, and application to tectonic settings. In: Holdsworth, R.E., Strachan, R.A., Dewey, J.F. (Eds.), Continental Transpressional and Transtensional Tectonics. Geological Society of London Special Publication, vol. 135, pp. 15–33.

Fynn, G.W., Powell, W.J.A., 1979. The Cutting and Polishing of Electro-optic Materials. Adam Hilger, London, 215 pp.

Gapais, D., Cobbold, P.R., 1987. Slip system domains. 2. Kinematic aspects of fabric development in polycrystalline aggregates. Tectonophysics 138, 289–309.

Ghosh, S.K., Ramberg, H., 1976. Reorientation of inclusions by combination of pure and simple shear. Tectonophysics 34, 1–70.

Giorgis, S., Tikoff, B., 2004. Constraints on kinematics and strain from feldspar porphyroclast populations. In: Alsop, G.I., Holdsworth, R.E., McCaffrey, K.J.W., Hand, M. (Eds.), Flow Processes in Faults and Shear Zones. Geological Society, London Special Publication, vol. 224, pp. 265–285.

Grasemann, B., Fritz, H., Vannay, J.C., 1999. Quantitative kinematic flow analysis from the Main Central Thrust Zone (NW-Himalaya, India); implications for a decelerating strain path and the extrusion of orogenic wedges. Journal of Structural Geology 21, 837–853.

Grover, T.W., Fernandes, L.C., 2003. Bedrock geology of the Weeks Mills 7.5′ quadrangle, Maine. Maine Geological Survey Open-File Map 03-49, Scale = 1:24,000.

Handy, M.R., 1994. The energetics of steady state heterogeneous shear in mylonitic rock. Materials Science and Engineering A174, 261–272.

Handy, M.R., Hirth, G., Bürgmann, R., 2007. Continental fault structure and rheology from the frictional-to-viscous transition downward. In: Handy, M.R., Hirth, G., Hovius, N. (Eds.), Tectonic Faults – Agents of Change on a Dynamic Earth, Dahlem Workshop Report 95. The MIT Press, Cambridge, Mass., USA, pp. 139–181.

Heilbronner, R., Tullis, J., 2002. The effect of static annealing on microstructure and crystallographic preferred orientations of quartzites experimentally deformed in axial compression and shear. In: de Meer, S., Drury, M.R., de Bresser, J.H.P., Pennock, G.M. (Eds.), Deformation Mechanisms, Rheology and Tectonics: Current Status and Future Perspectives. Geological Society, London Special Publication, vol. 200, pp. 191–218.

Holcombe, R.J., Little, T.A., 2001. A sensitive vorticity gauge using rotated porphyroblasts and its application to rocks adjacent to the Alpine Fault, New Zealand. Journal of Structural Geology 23, 979–990.

Hubbard, M.S., Wang, H., 1999. Temperature variability during shear deformation: an interpretation of microstructures along the central Norumbega fault zone, Maine. In: Ludman, A., West Jr., D.P. (Eds.), Norumbega Fault System of the Northern Appalachians. Boulder CO. Geological Society of America Special Paper, vol. 331, pp. 25–40.

Iacopini, D., Carosi, R., Montomoli, C., Passchier, C.W., 2007a. Strain analysis and vorticity of flow in the Northern Sardinian Variscan Belt: Recognition of a partitioned oblique deformation event. Tectonophysics 446, 77–96.

Iacopini, D., Passchier, C.W., Koehn, D., Carosi, R., 2007b. Fabric attractors in general triclinic flow systems and their application to high strain shear zones: a dynamical system approach. Journal of Structural Geology 29, 298–317.

Ildefonse, B., Mancktelow, N.S., 1993. Deformation around rigid particles: the influence of slip at the particle/matrix interface. Tectonophysics 221, 345–359.

Ildefonse, B., Launeau, P., Bouchez, J.L., Fernandez, A., 1992a. Effect of mechanical interactions on the development of shape preferred orientations: a two-dimensional experimental approach. Journal of Structural Geology 14, 73–83.

Ildefonse, B., Sokoutis, D., Mancktelow, N.S., 1992b. Mechanical interactions between rigid particles in a deforming ductile matrix. Analogue experiments in simple shear flow. Journal of Structural Geology 14, 1253–1266.

Jeffery, G.B., 1922. The motion of ellipsoidal particles immersed in a viscous fluid. Proceedings of the Royal Society of London A102, 161–179.

Jessell, M., Lister, G.S., 1990. A simulation of the temperature dependence of quartz fabrics. In: Knipe, R.J., Rutter, E.H. (Eds.), Deformation Mechanisms, Rheology and Tectonics. Geological Society of London Special Publication, vol. 54, pp. 353–362.

Jessup, M.J., Law, R.D., Searle, M.P., Hubbard, M.S., 2006. Structural evolution and vorticity of flow during extrusion and exhumation of the Greater Himalayan Slab, Mount Everest Massif, Tibet/Nepal: implications for orogen-scale flow partitioning. In: Law, R.D., Searle, M.P., Godin, L. (Eds.), Channel Flow, Extrusion, and Exhumation in Continental Collision Zones. Geological Society, London, Special Publications, vol. 268, pp. 379–414.

Jessup, M.J., Law, R.D., Frassi, C., 2007. The Rigid Grain Net (RGN): an alternative method for estimating mean kinematic vorticity number (Wm). Journal of Structural Geology 29, 411–421.

Jiang, D., 1998. Forward modeling of non-steady-state deformations and the 'minimum strain path': discussion. Journal of Structural Geology 20, 975–977.

Jiang, D., Lin, S., Williams, P.F., 2001. Deformation path in high-strain zones, with reference to slip partitioning in transpressional plate-boundary regions. Journal of Structural Geology 23, 991–1005.
Johnson, S.E., 2008. Numerical investigation of the effects of strain localization on rigid object kinematics. In: Bons, P.D.D., Koehn, D., Jessell, M.W. (Eds.), Microdynamics Simulation. Lecture Notes in Earth Science, vol. 106, pp. 247–253.
Kenkmann, T., Dresen, G., 1998. Stress gradients around porphyroclasts: palaeopiezometric estimates and numerical modeling. Journal of Structural Geology 20, 163–173.
Kronenberg, A.K., Kirby, S.H., Pinkston, J., 1990. Basal slip and mechanical anisotropy of biotite. Journal of Geophysical Research 95, 19257–19278.
Law, R.D., 1990. Crystallographic fabrics: a selective review of their applications to research in structural geology. In: Knipe, R.J., Rutter, E.H. (Eds.), Deformation Mechanisms, Rheology and Tectonics. Geological Society, London, Special Publications, vol. 54, pp. 335–352.
Law, R.D., Searle, M.P., Simpson, R.L., 2004. Strain, deformation temperatures and vorticity of flow at the top of the Greater Himalayan Slab, Everest Massif, Tibet. Journal of the Geological Society London 161, 305–320.
Law, R.D., Searle, M.P., Godin, L. (Eds.), 2006. Channel Flow, Extrusion, and Exhumation in Continental Collision Zones. Geological Society, London, Special Publications, vol. 268, p. 630.
Lin, S., Jiang, D., Williams, P.F., 1998. Transpression (or transtension) zones of triclinic symmetry: natural example and theoretical modeling. In: Holdsworth, R.E., Strachan, R.A., Dewey, J.F. (Eds.), Continental transpressional and transtensional tectonics. Geological Society of London Special Publication, vol. 135, pp. 41–57.
Lister, G.S., Hobbs, B.E., 1980. The simulation of fabric development during plastic deformation and its application to quartzite: fabric transitions. Journal of Structural Geology 1, 99–115.
Lister, G.S., Snoke, A.W., 1984. S-C mylonites. Journal of Structural Geology 6, 617–638.
Ludman, A., 1998. Evolution of a transcurrent fault zone in shallow crustal metasedimentary rocks: the Norumbega fault zone, eastern Maine. Journal of Structural Geology 20, 93–107.
Ludman, A., Lanzirotti, A., Lux, D.R., Wang, C., 1999. Constraints on timing and displacement of multistage shearing in the Norumbega fault system, eastern Maine. In: Ludman, A., West Jr., D.P. (Eds.), Norumbega Fault System of the Northern Appalachians. Geological Society of America Special Paper, vol. 331, pp. 179–194.
Ludman, A., West Jr., D.P. (Eds.), 1999. The Norumbega Fault System of the Northern Appalachians. Geological Society of America Special Paper, vol. 331, p. 199.
Mancktelow, N.S., Arbaret, L., Pennacchioni, G., 2002. Experimental observations on the effect of interface slip on rotation and stabilisation of rigid particles in simple shear and a comparison with natural mylonites. Journal of Structural Geology 24, 567–585.
Mariani, E., Brodie, K.H., Rutter, E.H., 2006. Experimental deformation of muscovite shear zones at high temperatures under hydrothermal conditions and the strength of phyllosilicate-bearing faults in nature. Journal of Structural Geology 28, 1569–1587.
Marques, F.O., Taborda, R., Bose, S., Antunes, J., 2005a. Effects of confinement on matrix flow around a rigid inclusion in viscous simple shear: insights from analogue and numerical modelling. Journal of Structural Geology 27, 379–396.
Marques, F.O., Taborda, R., Antunes, J., 2005b. Influence of a low-viscosity layer between rigid inclusion and viscous matrix on inclusion rotation and matrix flow: a numerical study. Tectonophysics 407, 101–115.
Marques, F.O., Schmid, D.W., Andersen, T.B., 2007. Applications of inclusion behavior models to a major shear zone system: the Nordfjord–Sogn Detachment Zone in western Norway. Journal of Structural Geology 29, 1622–1631.
Masuda, T., Michibayashi, K., Ohta, H., 1995. Shape preferred orientation of rigid particles in a viscous matrix: reevaluation to determine kinematic parameters of ductile deformation. Journal of Structural Geology 17, 115–129.
Means, W.D., Hobbs, B.E., Lister, G.S., Williams, P.F., 1980. Vorticity and non-coaxiality in progressive deformations. Journal of Structural Geology 2, 371–378.
Meyer, E.E., Greene, G.W., Alcantar, N.A., Israelachvili, J.N., Boles, J.R., 2006. Experimental investigation of the dissolution of quartz by a muscovite mica surface: implications for pressure solution. Journal of Geophysical Research 111, B08202. doi:10.1029/2005JB004010.
McKenzie, D., 1979. Finite deformation during fluid flow. Geophysical Journal of the Royal Astronomical Society 58, 689–715.
Mulchrone, K.F., 2007. An analytical solution in 2D for the motion of rigid elliptical particles with a slipping interface under a general deformation. Journal of Structural Geology 29, 950–960.
Niemeijer, A.R., Spiers, C.J., 2005. Influence of phyllosilicates on fault strength in the brittle-ductile transition: insights from rock analogue experiments. In: Bruhn, D., Burlini, L. (Eds.), High Strain Zones: Structure and Physical Properties. Geological Society of London Special Publication, vol. 245, pp. 303–327.
Osberg, P.H., Hussey, A.M. II, Boone, G.M. (Eds), 1985. Bedrock Geologic Map of Maine, Maine Geological Survey, Scale=1:500,000.
Passchier, C.W., 1986. Flow in natural shear zones – the consequences of spinning flow regimes. Earth and Planetary Science Letters 77, 70–80.
Passchier, C.W., 1987. Stable positions of rigid objects in non-coaxial flow – a study in vorticity analysis. Journal of Structural Geology 9, 679–690.
Passchier, C.W., 1988. Analysis of deformation paths in shear zones. Geologisches Rundschau 77, 309–318.
Passchier, C.W., 1997. The fabric attractor. Journal of Structural Geology 19, 113–127.
Passchier, C.W., 1998. Monoclinic model shear zones. Journal of Structural Geology 20, 1121–1138.
Passchier, C.W., Trouw, R.A.J., 2005. Microtectonics, second ed. Springer, 366 pp.
Pennacchioni, G., Fasolo, L., Cecchi, M.M., Salasnich, L., 2000. Finite element modeling of simple shear flow in Newtonian and non-Newtonian fluids around a circular rigid particle. Journal of Structural Geology 22, 663–692.
Pennacchioni, G., Di Toro, G., Mancktelow, N.S., 2001. Strain-insensitive preferred orientation of porphyroclasts in Mont Mary mylonites. Journal of Structural Geology 23, 1281–1298.
Piazolo, S., Bons, P.D., Passchier, C.W., 2002. The influence of matrix rheology and vorticity on fabric development of populations of rigid objects during plane strain deformation. Tectonophysics 351, 315–329.
Platt, J.P., Behrmann, J.H., 1986. Structures and fabrics in a crustal-scale shear zone, Betic Cordillera, SE Spain. Journal of Structural Geology 8, 15–33.
Robin, P.Y.F., Cruden, A.R., 1994. Strain and vorticity patterns in ideally ductile transpressional zones. Journal of Structural Geology 16, 447–466.
Samanta, S.K., Mandal, N., Chakraborty, C., 2003. Flow patterns around rigid inclusions in a multiple inclusion system undergoing bulk simple shear deformation. Journal of Structural Geology 25, 209–221.
Schmid, D.W., Podladchikov, Y.Y., 2005. Mantled porphyroclast gauges. Journal of Structural Geology 27, 571–585.
Schmidt, N.H., Olesen, N.O., 1989. Computer-aided determination of crystal lattice orientation from electron channeling patterns in the SEM. Canadian Mineralogist 27, 15–22.
Short, H.A., Johnson, S.E., 2006. Estimating vorticity from fibrous calcite veins, central Maine, USA. Journal of Structural Geology 28, 1167–1182.
Simpson, C., De Paor, D.G., 1993. Strain and kinematic analysis in general shear zones. Journal of Structural Geology 15, 1–20.
Simpson, C., De Paor, D.G., 1997. Practical analysis of general shear zones using porphyroclast hyperbolic distribution method: an example from the Scandinavian Caledonides. In: Sengupta, S. (Ed.), Evolution of Geological Structures in Micro- to Macro-scales. Chapman and Hall, London, pp. 169–184.
Sullivan, W.A., 2008. Significance of transport-parallel strain variations in part of the Raft River shear zone, Raft River Mountains, Utah, USA. Journal of Structural Geology 30, 138–158.
Swanson, M.T., 1988. Pseudotachylyte-bearing strike-slip duplex structures in the Fort Foster Brittle Zone, S. Maine. Journal of Structural Geology 10, 813–828.
Swanson, M.T., 1989. Sidewall ripouts in strike-slip faults. Journal of Structural Geology 11, 933–948.
Swanson, M.T., 1999. Dextral transpression at the Casco Bay restraining bend, Norumbega fault zone, coastal Maine. In: Ludman, A., West Jr., D.P. (Eds.), Norumbega Fault System of the Northern Appalachians Boulder CO. Geological Society of America Special Paper, vol. 331, pp. 85–104.
Swanson, M.T., 2005. Geometry and kinematics of adhesive wear in brittle strike-slip fault zones. Journal of structural Geology 27, 871–887.
Swanson, M.T., 2006. Pseudotachylyte-bearing strike-slip faults in mylonitic host rocks, Fort Foster Brittle Zone, Kittery, Maine. In: Earthquakes: Radiated Energy and the Physics of Faulting. Geophysical Monograph Series, vol. 170, pp. 167–180.
Takeshita, T., Wenk, H.R., Lebensohn, R., 1999. Development of preferred orientation and microstructure in sheared quartzite: comparison of natural data and simulated results. Tectonophysics 312, 133–155.
ten Grotenhuis, S.M., Passchier, C.W., Bons, P.D., 2002. The influence of strain localization on the rotational behaviour of rigid objects in experimental shear zones. Journal of Structural Geology 24, 485–499.
ten Grotenhuis, S.M., Trouw, R.A.J., Passchier, C.W., 2003. Evolution of mica fish in mylonitic rocks. Tectonophysics 372, 1–21.
Tikoff, B., Fossen, H., 1993. Simultaneous pure and simple shear: the unifying deformation matrix. Tectonophysics 217, 267–283.
Tikoff, B., Fossen, H., 1995. The limitations of three-dimensional kinematic vorticity analysis. Journal of Structural Geology 12, 1771–1784.
Tikoff, B., Fossen, H., 1999. Three dimensional reference deformations and strain facies. Journal of Structural Geology 21, 1497–1512.
Truesdell, C., 1953. Two measures of vorticity. Journal of Mechanics and Analysis 2, 173–217.
Tullis, J., 1977. Preferred orientation of quartz produced by slip during plane strain. Tectonophysics 39, 87–102.
Tullis, J., Christie, J.M., Griggs, D.T., 1973. Microstructures and preferred orientations of experimentally deformed quartzites. Geological Society of America Bulletin 84, 297–314.
Vissers, R.L.M., 1989. Asymmetric quartz c-axis fabrics and flow vorticity: a study using rotated garnets. Journal of Structural Geology 11, 231–244.
Wallis, S.R., 1992. Vorticity analysis in a metachert from the Sanbagawa Belt, SW Japan. Journal of Structural Geology 14, 271–280.
Wallis, S.R., 1995. Vorticity analysis and recognition of ductile extension in the Sanbagawa belt, SW Japan. Journal of Structural Geology 17, 1077–1093.
Wallis, S.R., Platt, J.P., Knott, S.D., 1993. Recognition of synconvergence extension in accretionary wedges with examples from the Calabrian Arc and the Eastern Alps. American Journal of Science 293, 463–495.
Wang, C., Ludman, A., 2003. Evidence for post-Acadian through Alleghanian deformation in eastern Maine: multiple brittle reactivation of the Norumbega fault system. Atlantic Geology 38, 35–51.

Wang, C., Ludman, A., 2004. Deformation conditions, kinematics, and evolution of shallow crustal ductile shearing in the Norumbega fault system in the northern Appalachians. Tectonophysics 384, 129–148.

Wenk, H.R., Canova, G., Molinari, A., Kocks, U.F., 1989. Viscoelastic modeling of texture development in quartzite. Journal of Geophysical Research 94, 17,895–17,906.

West Jr., D.P., 1999. Timing of displacements along the Norumbega fault system, south-central and south-coastal Maine. In: Ludman, A., West Jr., D.P. (Eds.), Norumbega Fault System of the Northern Appalachians. Geological Society of America Special Paper, vol. 331, pp. 167–178.

West Jr., D.P., Hubbard, M.S., 1997. Progressive localization of deformation during exhumation of a major strike-slip shear zone: Norumbega fault zone, Maine. Tectonophysics 273, 185–201.

West, D.P., Jr., Peterman, E.M., 2004. Bedrock Geology of the Razorville 7.5′ Quadrangle, Maine. Maine GeologicalSurvey Map 04-29, Scale 1:24,000.

West Jr., D.P., Roden-Tice, M.K., Potter, J.K., Barnard, N.Q., 2008. Assessing the role of orogen-parallel faulting in post-orogenic exhumation: low-temperature thermochronology across the Norumbega Fault System, Maine. Canadian Journal of Earth Sciences 45, 287–301.

Williams, P.F., Jiang, D., Lin, S., 2006. Interpretation of deformation fabrics of infrastructure zone rocks in the context of channel flow and other tectonic models. In: Law, R.D., Searle, M.P., Godin, L. (Eds.), Channel Flow, Extrusion, and Exhumation in Continental Collision Zones. Geological Society, London, Special Publications, vol. 268, pp. 221–235.

Xypolias, P., 2009. Some new aspects of kinematic vorticity analysis in naturally deformed quartzites. Journal of Structural Geology 31, 3–10.

Xypolias, P., Doutsos, T., 2000. Kinematics of rock flow in a crustal scale shear zone: implications for the orogenic evolution of the southwestern Hellenides. Geological Magazine 137, 81–96.

Xypolias, P., Koukouvelas, I.K., 2001. Kinematic vorticity and strain patterns associated with ductile extrusion in the Chelmos shear zone (External Hellinides, Greece). Tectonophysics 338, 59–77.

Xypolias, P., Kokkalas, S., 2006. Heterogeneous ductile deformation along a mid-crustal extruding shear zone: an example from the External Hellenides (Greece). In: Law, R.D., Searle, M.P., Godin, L. (Eds.), Channel Flow, Extrusion, and Exhumation in Continental Collision Zones. Geological Society, London, Special Publications, vol. 268, pp. 497–516.